REMOTE-SENSING DETECTION OF INVASIVE CHINESE TALLOW (*Triadica sebifera*) IN A FLOODPLAIN ENVIRONMENT

A Thesis

by

JAROM PERCY RANDALL

Submitted to the Office of Graduate and Professional Studies of
Texas A&M University
in partial fulfillment of the requirements for the degree of

MASTER OF SCIENCE

Chair of Committee.	Anthony M. Filippi
Committee Members.	İnci Güneralp
	William E. Rogers
Head of Department.	David Cairns

August 2015

Major Subject: Geography

ABSTRACT

Chinese tallow (*Tradica sebifera*) is an established invasive species in many southern woodlands in the United States. Its ability to adapt and spread quickly into disturbed areas has made it an invasive species of much concern to land managers. Riparian/floodplain environments have been affected by tallow as much as upland areas and entail a high degree of Chinese tallow invasion. Remote sensing is a tool that may provide a means of detecting, or classifying, Chinese tallow. There have been very few studies that have attempted to map Chinese tallow in a floodplain environment.

This research focused on mapping Chinese tallow on a single river meander bend. The purpose of this study was to determine which of the nonparametric detection methods considered, such as Multivariate Regression Splines (MARS), Stochastic Gradient Boosting (SGB) and the Random Forest (RF) models, as well as common spectral-extraction algorithms, were able to most accurately detect Chinese tallow in a floodplain forest based on remote-sensing data. In addition, it was the purpose of this study to attempt to determine factors affecting tallow growth and spread, and to map the spatial distribution of tallow in the study area.

Fieldwork was conducted in 2010 and 2014 to acquire Chinese tallow presence/absence information to be used for classification model training and testing. A hyperspectral Hyperion satellite image from summer 2010 constituted the primary remote-sensing data source, as well as airborne LiDAR data.

The three nonparametric models tested were used to predict Chinese tallow occurrences in the study area. A variety of input variables were employed in the modeling process, including: Hyperion image bands, dimensionality-reduced Minimum Noise Fraction (MNF) images, vegetation indices, and topographic and soil variables. An endmember-based approach was also used to classify tallow presence but was not very successful.

Results show that the most accurate dataset-combination trials involving both SGB and MARS yield high overall classification accuracy, 92.85%, whereas the most accurate RF dataset-combination trial provides lower overall classification accuracy, at 80%. Both spatial and aspatial statistical analyses were performed on the classification results. Significance testing indicates that the most accurate RF classification is not statistically significantly different from the most accurate SGB and MARS classifications. However, other error matrix significance testing finds the most accurate RF classification to be statistically significantly different from the most accurate SGB and MARS Chinese tallow classifications. A hot-spot analysis revealed that homogenous areas classified as tallow or as non-tallow can be detected and identified. Results from this study are promising in many areas of the meander bend, such as the transition zone where tallow is prevalent but less so in areas that have more established forest. Some methods tested were successful in detecting tallow and their use may aid land managers in the managing Chinese tallow growth and spread.

DEDICATION

This thesis is dedicated to my parents, Scott and Gayle, for teaching me to do what I want and to do the best I could to obtain it. To my sisters Tresa, Michelle and Valerie for their unfailing support, and to my wife Beth who was always by my side through some of the hardest parts of this adventure.

ACKNOWLEDGEMENTS

I wish to acknowledge the following people, without whose help and contributions this project would not have been possible:

Thank you to my chair Dr. Anthony Filippi and to my committee members Dr. İnci Güneralp and Dr. William Rogers for all of the advice they gave during this project.

Thank you to Sarah Nyikos, Dr. Güneralp, Dr. Filippi, and the team of supporting volunteers for performing the initial fieldwork in 2010.

Thank you to Stuart Marcus, Refuge Manager, Laurie Lomas Gonzales, Refuge Biologist, and the rest of the staff at the Trinity River National Wildlife Refuge office of the U.S. Fish and Wildlife Service in Liberty, TX, USA for providing local information on the Trinity River and logistical support, including the use of their facilities while performing fieldwork both in 2010 and 2014.

Finally, a big thank you to my fellow geography students Chris Maderia and Cesar Castillo for braving the jungle and helping me to conduct the additional fieldwork.

TABLE OF CONTENTS

LIST OF FIGURES

Page

LIST OF TABLES

Page

1. INTRODUCTION

Invasive plant species cause billions of dollars to be lost each year wide due to the loss of biodiversity, ecosystem modification, and mitigation efforts to prevent such changes. They have been, and continue to be a concern among scientists because of the modifications they make to the ecosystems they invade. Invasive plants spread through various means but many more noxious plants have been spread via humans. Reasons for spreading these plants are usually not malicious but large consequences have been observed. Indeed, invasive plants are one of the most significant modifications humans have made on the landscape. (Vitousek et al. 1997).

Chinese tallow (*Triadica sebifera)* is one of the most significant invasive plants in the southeastern United States (Bruce, Cameron and Harcombe 1995, Burns and Miller 2004, Wang et al. 2011). Estimates as of 2008 indicate that 185,000 hectares of forests are occupied by Chinese tallow, and that its range is still increasing (Gan et al. 2009, Wang et al. 2011). Chinese tallow has been shown to be highly adaptable to its environment and its range is only restricted due to cold temperatures, extremely wet conditions such as areas dominated by flooding, and overstory shade (Pattison and Mack 2009, Rogers and Siemann 2003, Butterfield, Rogers and Siemann 2004, Nijjer et al. 2002, Zou, Rogers and Siemann 2009). It tends to colonize low, flat and more moist areas and colonizes more quickly in disturbed areas and areas with more open canopies (Bruce et al.

1995, Burns and Miller 2004, Pattison and Mack 2009, Rogers and Siemann 2003).

Riparian ecosystems are important to the global carbon cycle and are one of the most diverse ecosystems (Rosenberg, McCully and Pringle 2000). Riparian ecosystems along meandering rivers are very dynamic due to the movement of the river (Perucca, Camporeale and Ridolfi 2007). The movement of the river can create disturbance zones in these riparian areas which are susceptible to invasion (Sher, Marshall and Gilbert 2000).

Remote sensing is a highly utilitarian tool for mapping and monitoring change in riparian environments (Filippi, Güneralp and Randall 2014, Güneralp, Filippi and Randall 2014b, Güneralp, Filippi and Hales 2014a, Güneralp, Filippi and Hales 2013). Once a procedure has been established to classify and map features on the landscape, the multi-temporal nature of remote sensing makes it possible to track those features through time (Coppin and Bauer 1996). Using the spectral information inherent in remote-sensing images, it may be possible to detect/classify Chinese tallow in a riparian environment. Few studies have attempted to classify Chinese tallow based on remote-sensing images (Ramsey III et al. 2005c). Ramsey III et al. (2005a – 2005c) are the main existing using remote sensing to detect Chinese tallow, which do not utilize remote-sensor images acquired during the summer, and the focus is not on riparian areas.

Many aspects of riparian systems are variable and nonlinear such as flooding regimes, vegetation dynamics, and meander migration(Camporeale and

Ridolfi 2010, Camporeale and Ridolfi 2006, Güneralp and Rhoads 2009, Güneralp and Rhoads 2010, Güneralp and Rhoads 2011). The nonlinear nature of riparian environmental systems in general necessitates the use of nonparametric methods when classifying remote-sensing images (Phillips 1992). Methods such as Multivariate Adaptive Regression Splines (MARS) and Stochastic Gradient Boosting (SGB) have only very rarely been utilized in a species-specific remote-sensing classification. These algorithms have a variety of different advantages, which include using variable interactions that can be fitted into the model allowing for a more dynamic interaction between predictor variables, stochastic modeling eliminating the need to pre-select variables and a resistance to overfitting. These advantages make them ideal for this kind of a study and may make them useful in detecting/classifying Chinese tallow (Friedman 2002, Friedman 1991). In addition, more established hyperspectral image-processing methods, such as image endmember extraction and spectral unmixing algorithms, may yield useful results, given the spectral resolution of hyperspectral images.

This study employs remote-sensor image data and a variety of classification methods to detect/classify Chinese tallow in a riparian environment. Both multispectral and hyperspectral images are used in these classifications, as well as a variety of ancillary variables. This research aims to identify the most accurate remote-sensing image-processing method for classifying Chinese tallow, of the algorithms evaluated. The research questions

of this study are: 1) Can remote sensing be used to accurately detect Chinese tallow trees during deciduous forest summer (leaf-on) conditions?; 2) Which algorithm/dataset combinations are optimal in detecting Chinese tallow?; and 3) Can the spatial distribution of tallow be examined using spatial statistics? These questions lead to several research objectives. The objectives of this research are: 1) to detect and map Chinese tallow in a floodplain forest using summer hyperspectral satellite image and other data, as well as nonparametric modeling and spectral unmixing/matching techniques; 2) to determine algorithm/dataset combinations that yield the highest-accuracy Chinese tallow classifications, of the detection algorithms and input variables tested; and 3) to quantitatively characterize the spatial distribution of Chinese tallow trees.

2. LITERATURE REVIEW AND BACKGROUND

2.1 Chinese tallow as an invasive species

2.1.1 Characteristics of **Triadica sebifera** *(Chinese tallow)*

Chinese tallow has many names by which it is referred, i.e., Chinese tallow, tallow tree, popcorn tree, Florida aspen, and chicken tree (Jubinsky and Anderson 1996). It is a member of the Spurge family, and is generally accepted to be poisonous. It starts to flower when it is around three feet high (Godfrey 1988). The leaves are simple in structure, which are broader than they are long, the blades are rhombic, and ~3-7 cm in length. The leaves also have glands at the blade-petiole junction that in the late summer and early fall will exude a sugary fluid (Correll and Johnston 1970). The fruit is usually found in groups of three lobes, with a seed in each lobe. The fruit dehisces in the autumn to leave three white seeds that stay attached to the tree; these seeds, which then look like popcorn, are the reason for one of its names, the popcorn tree. The tree type ranges from a low-spreading tree with forked branches to a taller columnar tree with pendant branches (Jubinsky and Anderson 1996).

Chinese tallow generally inhabits wetter lowland areas, and may be further dispersed via water corridors. It also can be found in upland areas, but is not as prevalent in such environments (Pattison and Mack 2009). Indeed, it has often been found in low, flat areas adjacent to water bodies and roads, and it is not as prevalent in more mature stands of forest (Wang et al. 2011, Bruce et al. 1995, Ramsey III et al. 2005c). There do not seem to be many factors that limit

the growth of Chinese tallow. The primary factor that may limit its growth is temperature, but that is not a factor in the present study, as the study area is very small and therefore temperature does not vary much over the study site. A larger geographical scale would factor in temperature into its analysis. Furthermore, the spatial extent of the study area is rather limited, and the spatial variability of temperature across the study area is thus also limited. Pattison and Mack (2009) found that one of the few other variables limiting tallow growth is the degree of openness of the canopy. In the study area for this research, the largest instances of tallow are in a transition zone where light is variable throughout the day and is an ideal amount of light for tallow to grow. Whereas tallow is sometimes present in closed-canopy environments, it has much more limited growth and distribution in such areas. Competition for and availability of nitrogen also seem to limit its expansion, but do not prevent its establishment and growth (Pattison and Mack 2009). Tallow is not negatively affected by herbivory either; it has shown to be extremely resistant to herbivory, and has a very high regrowth rate (Rogers and Siemann 2003). Areas with soils containing higher amounts of nitrogen may be more prone to tallow invasion (Rogers and Siemann 2003, Zou et al. 2006).

Figure 1 - Images of Chinese tallow tree, its leaves, and fruit. (Image source: http://www.cnseed.org/).

2.1.2. History and range expansion of Chinese tallow

Tallow (Figure 1) is native to eastern Asia, and mainly inhabits the same latitudes in the United States as those where it is found in Asia. It was introduced into the United States in the late eighteenth century, and was initially grown to make wax and oil from the fruit (Howes 1949). In that time, the species

has gradually spread throughout much of the southeastern part of the country, and has been found in California as well.

According to the United States Department of Agriculture (USDA 2014), it has not expanded further north than North Carolina, but it is still spreading throughout its range in the south. Multiple studies have found that it is continually expanding through the western part of its range and further north in Arkansas (Pattison and Mack 2009, Wang et al. 2011).

2.2 Riparian vegetation systems

2.2.1 Characteristics of riparian vegetation in a floodplain environment

Although this study is primarily focused on remote-sensing detection/classification of Chinese tallow, which is an invasive species in the United States, the environment in which the study is conducted plays a significant part in the growth of Chinese tallow and its spatial distribution (Butterfield et al. 2004). In addition, the present research contributes to the growing literature regarding tallow in riparian environments.

Riparian vegetation regimes are different from other environmental regimes due to the spatio-temporal dynamics among a variety of environmental factors and systems, as well as the inherent stochastic nature of riparian systems (Naiman, Decamps and McClain 2010). Some of these dynamics include: climatic controls, species types, disturbance regimes, and hydrologic and geomorphological controls (Richardson et al. 2007, Shafroth, Stromberg

and Patten 2002, Hupp and Osterkamp 1996). These riparian dynamics all vary significantly throughout the world, which may necessitate study of riparian systems at a more local or regional level that is associated with one type of morphological scale (van Coller, Rogers and Heritage 2000, Cooper, Andersen and Chimner 2003).

Biological diversity within riparian areas tends to be relatively high. This is a result of the frequently-changing water flows that characterize riparian areas. Flooding and topographic changes lead to changes in the interactions and exchanges between habitats. This biological diversity is often one of the factors that lend riparian areas to being so susceptible to invasion (Naiman et al. 2010).

In addition to hydrogeomorphic processes, the capability of a site for supporting establishment of particular species plays a role in the type of vegetation regime that is established. Factors that may affect this site capability include disturbances such as periodic flooding, sediment deposition, and soil properties. The interaction of these many factors translates to riparian environments being very stochastic in nature. This stochasticity leads to dynamic changes in vegetation regimes and makes riparian environments very susceptible to invasion (Hupp and Osterkamp 1996).

2.2.2 Vegetation invasion in riparian environments

Riparian systems are prone to invasion because of their dynamic nature, and the ability of streams and rivers to disperse propagules (Planty-Tabacchi et al. 1996, Pysek and Prach 1993). Flooding events can clear space for invasive species, and drought events may expose more soil for colonization (Thébaud and Debussche 1991). Many invasive species are adept at colonizing these types of spaces.

Anthropomorphic changes, such as dam construction or removal of a dam, may cause disturbances down- or up-river, which may trigger vegetation invasions (Shafroth et al. 2002). These invasions most often occur along stream and river banks. Often, more mature forest stands are more resistant to vegetation invasion because they have more established root systems and can outcompete species for light. However, such properties do not make them immune to invasion (Ward 2002).

2.3 Remote sensing and classification of invasive vegetation

2.3.1 Remote sensing of invasive vegetation

Remote sensing is a potentially useful tool for monitoring invasive vegetation species. Because of the multitemporal observation capabilities of orbital and suborbital remote-sensing systems, it is possible to monitor native and non-native species, including changes in their composition and spatial extent over time (Nagendra et al. 2012). There are also a variety of limitations

with this approach. Spectral, spatial radiometric, and/or temporal resolutions of spaceborne or airborne remote sensors may not be adequate to effectively map individual species or types of vegetation. The presence of clouds may inhibit the acquisition of good-quality images (passive images, in particular), and this may occur more during certain times of the year. Despite these limitations, remote sensing remains a potentially viable avenue for mapping invasive species.

To-date, the most successful use of remotely-sensed data to map invasive species has been with hyperspectral images. Hyperspectral images entail markedly higher spectral resolution than more common multispectral sensors such as Landsat, SPOT, or Quickbird (Hestir et al. 2008). Hyperspectral images thus often provide richer data sets from which identification of specific vegetation species or types of plants can be derived (Filippi and Jensen 2006). The majority of invasive-species studies involving remote sensing have utilized hyperspectral sensors, and they have found remote sensing to be effective in many cases (Andrew and Ustin 2009, Andrew and Ustin 2008, Hestir et al. 2008, Lawrence, Wood and Sheley 2006, Pengra, Johnston and Loveland 2007, Underwood, Ustin and DiPietro 2003, Ustin et al. 2002, Ramsey III et al. 2005c).

Multispectral images are not as utilized as frequently as their hyperspectral counterparts in identifying invasive species, but they may still provide some useful results in certain contexts. Many conventional multispectral satellite sensors, such as Landsat Thematic Mapper (TM)/Enhanced Thematic Mapper Plus (ETM+), Satellite Pour l'Observation de la Terre (SPOT), and

Advanced Spaceborne Thermal Emission and Reflection Radiometer (ASTER) entail relatively coarse spatial resolutions (e.g., 10–30 m). If the vegetation species of interest occurs in larger stands or patches, then multispectral images may be useful, but if trees of the species of interest are more sparsely distributed, spatially, then multispectral images may not prove useful for detection (Cho-ying and Asner 2009), particularly given the moderate spatial resolutions of such spaceborne sensors. Nonetheless, some studies have achieved some success using multispectral images (Groeneveld and Watson 2008, Narumalani et al. 2009).

2.3.2 Remote sensing of Chinese tallow

There currently is very little research regarding remote-sensing detection of Chinese tallow. A set of papers by Ramsey III and collaborators detail the classification of tallow using two different types of remote-sensor images, and several different techniques (Ramsey III et al. 2002, Ramsey III and Nelson 2005a, Ramsey III et al. 2005b, Ramsey III et al. 2005c). Other than the studies by Ramsey III et al., there is extremely limited research on using remote sensing to identify Chinese tallow. There are some limitations regarding this task, but there are also substantial benefits to successfully deploying a remote-sensing approach. These limitations may include low spatial resolution 30-m of the source imagery, difficulty separating tallow spectra from other vegetation spectra, and the mixed pixel problem. If a viable remote-sensing method for

identifying tallow can be found, then it will make it easier for land managers and others to identify and manage/control/eradicate tallow.

One of the distinct characteristics of Ramsey's methods is that he and his collaborators mapped tallow in the fall when it is senescing. Tallow has distinct red leaves when it is senescing, which makes it easier to identify, relative to other proximal trees. Ramsey hypothesized that it is much more feasible to identify tallow during the fall months when it is senescing and much of the other surrounding vegetation is not (Ramsey III and Nelson 2005a, Ramsey III et al. 2002, Ramsey III et al. 2005c, Ramsey III et al. 2005b). However, such a methodology that relies on exploiting color/spectral differences between senescent and non-senescent vegetation in the fall will likely only be effective in certain regions where such differences exist in the fall. For example, in areas of the United States further north within the current spatial extent of Chinese tallow, other forest tree species (e.g., native species) will also senesce with leaf color changes similar to that of Chinese tallow, complicating tallow detection.

Ramsey's first paper (Ramsey III et al., 2002) used high spatial-resolution color infrared aerial photography and a K-means clustering algorithm. This algorithm is an unsupervised algorithm that is meant to separate the various endmember spectra from one another to map individual occurrences of Chinese tallow. Although the spectral resolution of the imagery analyzed was low, there was sufficient spectral difference between the tallow and the surrounding vegetation for tallow detection because of the time of year the image data were

obtained. The red tallow leaves were distinct enough so that the tallow trees could be effectively identified. In addition to the geographical limitation noted above, one issue with this work is that the temporal window for obtaining an image with these spectral differences is small, and it often does not occur at the same each year. Nevertheless, Ramsey III et al. achieved favorable results using the image type and method.

Ramsey III's other study (Ramsey III and Nelson 2005a, Ramsey III et al. 2005b, Ramsey III et al. 2005c) is a series of papers detailing one project that implemented a method for utilizing hyperspectral imagery from the Hyperion sensor on the EO-1 platform to map tallow. Hyperion has a 30-m spatial resolution, which is likely coarser than ideal for detecting tallow, as in general large stands of tallow often do not exist together (Ramsey III et al. 2002). The first two papers (Ramsey III and Nelson 2005a, Ramsey III et al. 2005b) detailed his method for obtaining accurate spectra from Hyperion satellite imagery using an atmospheric correction method developed by Ramsey III, and an endmember approach that was able to retrieve four different tallow endmembers based on their stage of senescence. The third paper (Ramsey III et al. 2005c) documented his method for exploiting these spectra via sub-pixel detection of tallow. Approximately 81% (n=34) of the field- and 78% (n=33) of the Hyperion image-based characteristic spectra associated with 'red tallow' were explained by the compositions generated in the field site classifications. This approach was successful in quantifying the percentages of tallow in moderate spatial-resolution

Hyperion pixels and correlating those occurrences with pre-existing land-cover classifications for the study area of interest. Red tallow occurrences (10%) were detected 68% of the time and yellow tallow occurrences (15%) were detected 85% of the time.

Although the authors achieved some successful results in Ramsey III et al. (2005a – 2005c), there are some issues with the method of detecting tallow when it is senescing, which the authors acknowledge. Not all of the plants senesce at the same rate, which makes identifying tallow endmembers from the image spectra difficult. In Ramsey III et al. (2005a – 2005c), it was attempted to classify the vegetation in different stages of senescence, and then identify the tallow within those different stages. This approach makes it difficult to repeat this kind of analysis because every year the various tallow trees may senesce at different rates and at slightly/somewhat different times. Obtaining remote-sensing images during the correct/optimal time can be problematic. Furthermore, as noted above, there are geographical constraints on the applicability of this method based on spectral differences between senescent and non-senescent vegetation in the fall.

Whereas there are problems with the method proposed in Ramsey III et al. (2005a – 2005c), there are also some distinct advantages. Again, it is much easier to distinguish the tallow from other vegetation during the fall months, assuming that the remote detection is conducted in geographical areas where such distinct spectral differences exist in the fall, whereas in the summer

months, it may be difficult to distinguish Chinese tallow spectra from the spectra of other green vegetation. As Ramsey III et al. (2005a-2005c) note, although tallow is prevalent in many areas, it does not usually grow in large stands; therefore if the spatial resolution of the imagery is not very high, it will necessitate some kind of sub-pixel analysis. However, pure or relatively pure tallow pixels may not exist in a given moderate-spatial resolution image, which would affect the quality of image-derived tallow endmembers, and (field- or image-based) endmembers of the respective vegetation species within a study region may not be unique enough to enable discrimination between tallow another other species.

Often, remote-sensor images are more available for summer months than for winter months (Brandtberg et al. 2003), and although it could be more difficult to distinguish between Chinese tallow and non-Chinese tallow tree species during the summer, most trees will be relatively healthy and not in different stages of senescence, as was the case in Ramsey III et al. (2005 – 2005c). If tallow can be accurately mapped based on summer remote-sensing images, it may facilitate the ability of land managers to determine the spatial distributions of tallow, so that they can inhibit its spread.

3. STUDY AREA

The study site (Figure 2) consists of a single meander bend of the Lower Trinity River, a meandering river in East Texas; the study-area meander bend is located at 30° 08' 02" N, 94° 49' 02" W, approximately 9 km north of Liberty, Texas, USA. Aerial photography acquired over the past 60 years documents that the meander bend has exhibited a significant degree of migration and has rotated southward from its prior location in 1938.

The study site is on private property that has been used for light cattle grazing and was recently purchased by a logging company; however that company does not have long-term plans to log the area. Detailed cattle-grazing records for the study area are unavailable, and there is no information to suggest that cattle grazing has had any significant effect on vegetation pattern, structure, or community composition in the area. There is also some control on the wildlife population through hunting.

The study area is located entirely within the broad floodplain of the lower Trinity River, although in recent years the site has been unflooded or only partly flooded in some areas close to the active channel, most likely due to recent intense droughts (particularly May 2010 to March 2011, the time interval over which the majority of fieldwork was conducted). This assumption is based upon analysis of recent aerial imagery from the National Agriculture Imagery Program (NAIP) and previous gauge data. There have been some major flooding events where the entire study area has been flooded in the last 10 years (Personal

communication, Stuart Marcus USFWS). The Trinity River basin services two major metropolitan centers (Dallas and Houston), and has also undergone regulation of flow through the placement of the Livingston dam, located approximately 58 km NNW and approximately 107 km upstream of the study-area meander bend, and was constructed in 1966-1969 by Forest and Cotton, Inc.

Land-cover types at the site consist mainly of mature forest, grading to smaller trees and shrubs, and then to herbaceous vegetation progressively

Figure 2 - Study area location: a) southeastern Texas including Galveston Bay, Houston, and Liberty b) Trinity river north of the town of Liberty c) Meander bend that comprises the study area for this study located at at 30° 08' 02" N, 94° 49' 02" W

closer to the point bar. The forest appears from both multitemporal aerial image analysis and also field observation to have remained predominantly undisturbed for the most part at least the last sixty years; a small portion of the mature forest is likely first-growth. The tree community can be described as bottomland mixed hardwoods, or Southern Bottomland Forest, which are located in East Texas river bottomlands. Dominant species on this site are American sycamore (*Platanus occidentalis*), hackberry (*C. occidentalis*), roughleaf dogwood (*Cornus drummondii*), *L. styraciflua*, and in the mature forest, *P. deltoides* as well. Chinese tallow (*Triadica sebiferum*) is a non-native species that is pervasive throughout the site and is the focus of this study; it exists in all but the driest areas with high sun exposure and some of the more mature forest areas. Two species of water oak (*Q. nigra)* and willow oak (*Q. phellos)*, are found in a few areas, as well as a few individuals of the genus *Pinus*, specifically loblolly (*P. taeda*) and longleaf (*P. palustris*) pines. The area has experienced limited or no logging since at least 1938, based on analysis of multitemporal aerial photographs. Elevation across the site varies between 6 m above sea level at the edge of the active river channel to 10.3 m at the highest point, which is located on the northern cutbank of the site in the mature forest.

Soil across the site is fine alluvial sediment, and ranges from loamy fine sands (≥ 50 percent fine sand) to silty clays (total of ≥ 40 percent clay and ≥ 40 percent silt). Grain sizes range from coarse sand (≥ 1 mm) to very fine clay (< 0.02 µm)(Nyikos 2011). Soil data were later transformed into percent sand, silt, and clay surfaces for use in modeling.

Figure 3 - Chute intersecting the study area and along which the highest portions of tallow can be found. (True-color image source – National Agriculture Imagery Program (NAIP), 2008.)

The site is partially transected by an inlet or chute cut of the river, running approximately halfway across the site, in a northwest-trending direction (Figure. 3). This chute is important because the largest amounts of Chinese tallow tend to grow along this chute. The inlet also has a small sub-branch. This inlet enables water to periodically reach the interior of the site, except during extreme drought conditions, when the level of the river drops below the elevation of the inlet. (Drying of the inlet was observed on three separate visits to the site, in September 2010, March 2011 and June 2014, respectively.) However, the level of the river also changes periodically/continuously.

4. METHODS*

4.1 Fieldwork

4.1.1 Primary fieldwork

The initial fieldwork (Figure 4) was conducted by Sarah Nyikos (and Dr. İnci Güneralp, Dr. Anthony Filippi, and a team of supporting volunteers) preparation for her thesis work studying the tree community patterns on this meander bend (Nyikos 2011).The locations of the plots for data collection (Figure 4) were determined based on a coordinate grid (UTM NAD 1983); the exact location of the grid on the bend was determined through preliminary aerial photograph examination of vegetation pattern zonation. Grid lines were laid roughly parallel to the meander bend and the direction of channel migration, i.e., perpendicular to the apex of the channel bend. Grid mesh sizes were varied (100 m, 50 m and 25 m) to better incorporate the natural variability of the vegetation, particularly variation in above ground biomass. Plots were located approximately at the intersections of the lines of this grid; however, some plot locations were varied based on perceived zonation from preliminary visual interpretation of aerial imagery. In the field, both during 2010 and 2014 field data-collection campaigns, a Garmin® GPS unit was used for navigation to the plots locations, as well as for determining locations of center points and quadrats. Measurement of plot radii was performed using survey tapes. It was also necessary to move some plots slightly in the field from their anticipated

*Part of the data reported in this section reprinted from I*nternational Journal of Applied Earth Observation and Geoinformation*, 33, Güneralp, İ., A. M. Filippi & J. Randall, “Estimation of floodplain aboveground biomass using multispectral remote sensing and nonparametric modeling”, 119-126, Copyright 2014 with permission from Elsevier

locations as a result of the impenetrability of some vegetation; impenetrability also would have prevented the application of the transect method, had it been selected.

Initial primary fieldwork was conducted from mid-June to late September of 2010, with an additional visit to the site in mid-March 2011. Fieldwork involved the collection of detailed data on vegetation establishment (i.e., tree density, saplings, and seedlings) and sediment characteristics (i.e., grain size/ texture distribution) of the meander bend. Vegetation data collection methods included: measuring tree diameter at a standard breast height (dbh) of 1.3 to 1.4 m; identifying all tree species; counting and identifying saplings and tree seedlings. These three stages (trees, saplings and seedlings) reflect the various stages of tree establishment and growth/development. For the purposes of this study, trees were defined as having a dbh of ≥ 5 cm, saplings as being less than 5 cm but greater than 1 cm, and seedlings as < 1 cm dbh (Chambless and Nixon 1975) and also less than 0.5 m in height.

Thirty-two ~400 m^2 circular plots were established in 2010 on the study site (with radius of 11.3 m) (Figure 4). Within each plot, a smaller ~100 m^2 plot (with radius of 5.6 m) for sampling of saplings was centered. Two 1-m^2 quadrats within the main plot were used to sample seedlings. These were arbitrarily located at the north and south ends of each plot. Location of plots was based on coordinate grid. Note that some plots were moved very slightly in the field, but this is an accurate representation of their respective location.

Within each main plot, a soil sample was collected to be analyzed for grain-size variation. Samples were taken to a depth of 10 cm where possible; this has been indicated to be a suitable depth for seedling establishment (Robertson and Augspurger 1999). However, in many instances it was not possible to take samples below 5 cm.

Leaf litter was cleared from the ground surface before the samples were collected, and any large pieces of organic debris in the soil were removed in the field. Soil samples were then stored in airtight plastic bags until processing. Samples were analyzed to determine grain-size distributions and gradients across point bars. These samples were used to derive rasters for each of the soil texture characteristics used in model development.

4.1.2 Supplementary fieldwork and image-interpreted sample data

Additional fieldwork was performed June on10 and 11 June 2014 (Figure 4). The purpose of this supplementary data collection was to obtain counts of Chinese tallow trees in additional plots within the meander-bend study area. These additional data were collected to augment training and testing datasets for the nonparametric model development. Three transects were used to direct where field plots should be located (personal communication, W. E. Rogers, 2014). A single transect was first located along a transitional zone that may have formed due to disturbances such as meander migration, flooding and the presence of the chute that partially transects the study area. This area was

chosen because it contained the highest counts of Chinese tallow trees, as observed in the first series of field site visits, and it was hypothesized that obtaining more field data in this floodplain environment would help aid in developing more accurate tallow-detection models. Two additional transects were positioned 50 m from and parallel to the initial transect.

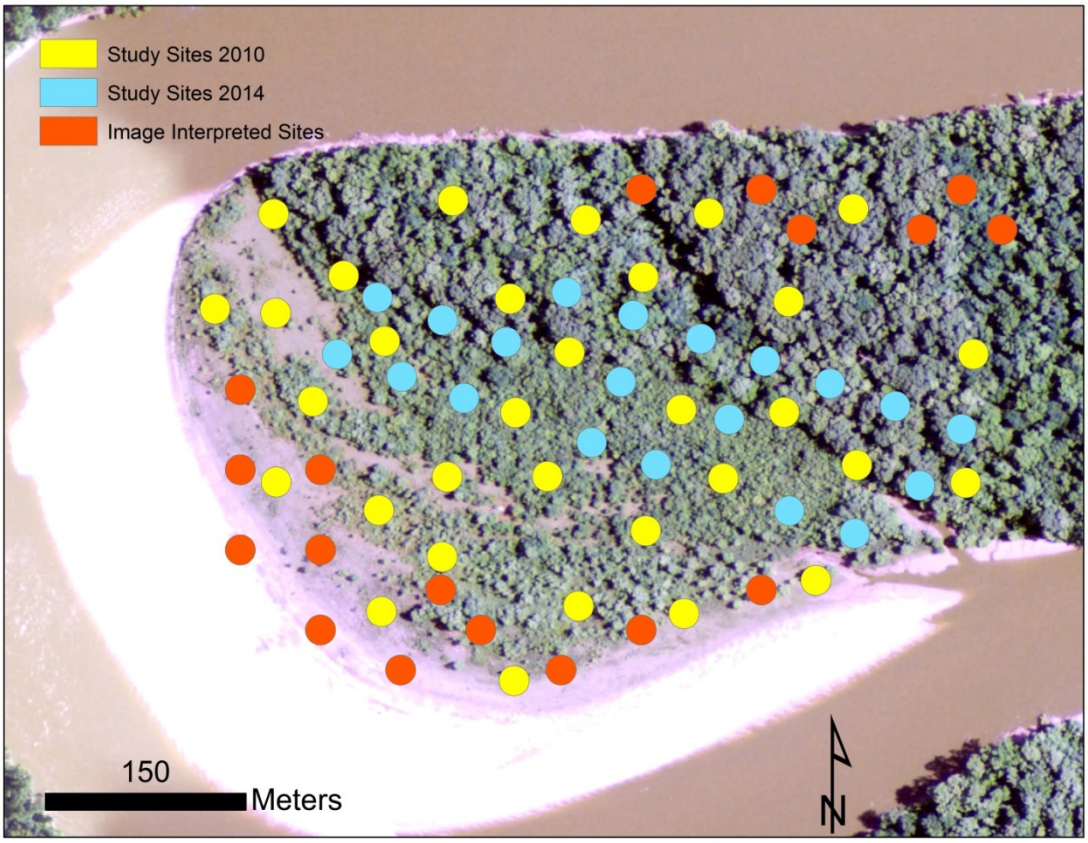

Figure 4 - Field sites and image-derived value locations. Locations for 2010 (yellow) and 2014 (blue) are shown with circles that are representative of the actual field plot size. The image-interpreted values (orange) are representative of the general area that a given circle occupies and were used only to provide more Boolean tallow/non-tallow information. (True-color image source – National Agriculture Imagery Program (NAIP), 2008.)

Along each of the transects, seven additional plots were located 30 m apart from edge-to-edge when possible. When other plots from the previous fieldwork were co-located with a potential new field plot, they were treated as an additional plot, and new plots were established at least 30 m away from them (Figure 4). These plots were exactly the same size as previous plots (400 m^2), and demarcated using similar techniques (via survey tapes). In the field, we navigated to the center points of each plot using a Garmin® gpsmap 78 GPS.

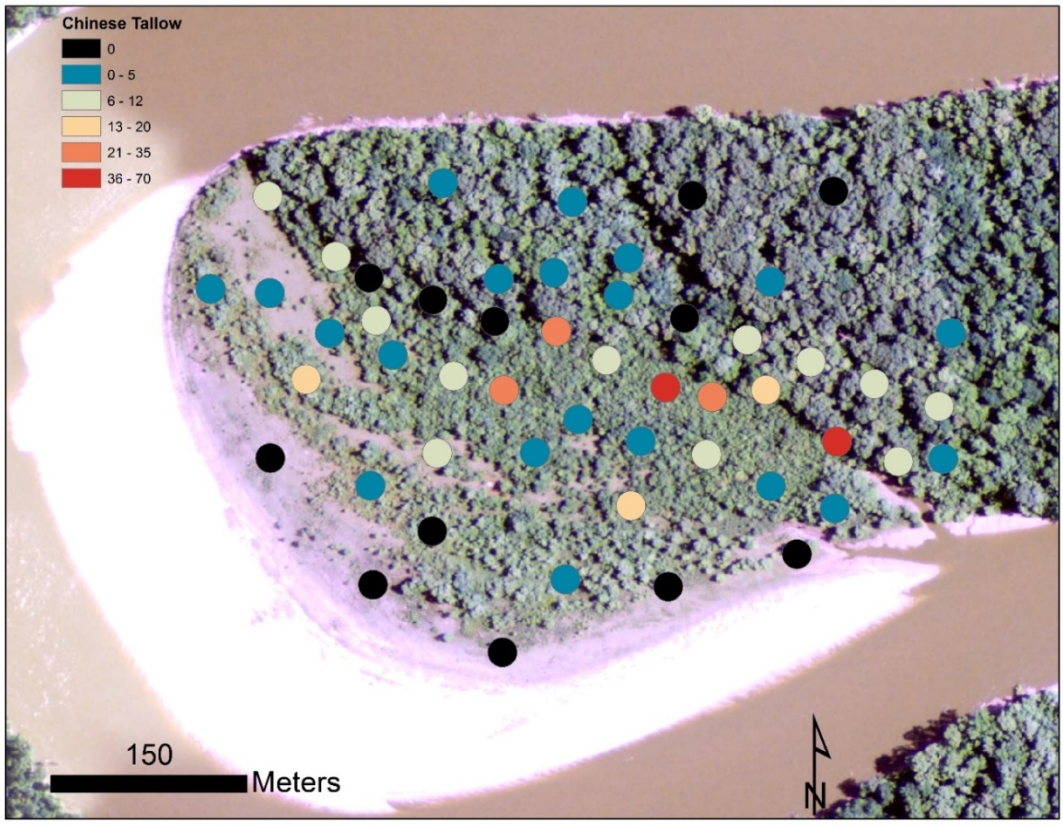

Figure 5 - Total number of tallow trees in field plots from both 2010 and 2014. Black circles indicate no presence of tallow in that field site. (True-color image source – National Agriculture Imagery Program (NAIP), 2008.)

Once the plots were established, the number of Chinese tallow within each plot was counted (Figure 5). As with the previous fieldwork, trees were defined as having a dbh > 5 cm. Number of tallow samplings was often noted in the field notes, but exact numbers were not counted. Although there was a four-year time span in between these two data-collection periods (Figure 4), we assume that the time difference is not markedly/significantly deleterious to field reference dataset construction, as these data were primarily used in this study for determining Chinese tallow presence/absence. Additionally, even though some of the tallow trees counted as trees in 2014 may have been saplings in 2010, there were, in most cases, multiple trees at each site that contained tallow and most likely would have been classified as trees in 2010.

Initial model results revealed that more data were necessary to effectively train and test the nonparametric models. These additional data were provided via image interpretation and previous knowledge of the study area. The nonparametric models predict Boolean results for whether or not a given pixel contains tallow trees. Thus, for these additional image-interpreted sites (Fig. 4), in order to accrue further Chinese tallow presence/absence information, it was only necessary to determine sites that most likely entail relatively high numbers of tallow trees, or almost certainly do not contain tallow trees, based on manual/visual image interpretation of aerial photography and hyperspectral Hyperion and multispectral SPOT satellite images, combined with *in situ* knowledge of the study area.

4.2 Hyperion image variable processing

4.2.1 Spectral and geometric correction

Spectral data were collected via hyperspectral Hyperion satellite image acquisition (30-m ground sample distance (GSD); 242 channels; acquired on 25 July 2010; 16:45:23 GMT). Hyperion image collection was temporally synchronized with the 2010 field data collection. Uncalibrated and spectral overlap bands were discarded, resulting in 196 unique bands. Hyperion atmospheric correction was performed using Atmospheric COrrection Now (ACORN™) code, Version. 5.1(ImSpecLLC 2004) to invert radiance to apparent surface reflectance (mode 1.5; mid-latitude summer model; 940 and 1140 nm water-vapor derivation; path radiance in spectral fit; baseline visibility = 20.64 km; ACORN estimated visibility; Types 1, 2 and 3 artifact suppression). High-noise bands were then removed (78–82, 97–100, 116, 118–133, 152–153, 165–182, 184–186 and 220–224), determined via signal-to-noise ratio (SNR) calculations and visual inspection. In addition, there were a number of bands that contained excessive striping and were removed (9-12, 101, 134, 164, 183, 187-197, 199-203, 205-206, 219) resulting in a final 115 band set (Table 1). Following spectral and spatial subsetting, a geometric correction was conducted with 50 ground control points (GCPs) and a second-order polynomial model (RMSE = 8.1 m).

Bands	Wavelengths (nm)
8	426.82
13-56	477.69-915.23
83-96	972.99-1104.19
102-115	1164.68-1295.86
117	1316.05
135-163	1497.63-1780.09
198	2133.24
204	2193.73
207-218	2224.03-2335.01

Table 1 - Final Hyperion bands used in model development and spectral analysis, comprising 115 bands in total.

4.2.2 Image dimensionality reduction

Two data dimensionality-reduction algorithms were applied separately to the Hyperion image to minimize potentially redundant information, given the highly-correlated bands. In this study, the aim was to test whether dimensionality-reduction improved Chinese tallow-detection accuracy. Specifically, minimum noise fraction (MNF) transform (Green et al. 1988) was one dimensionality-reduction method used. MNF is used to identify and

segregate noise, and then collapse useful bands into smaller sets of images (Green et al. 1988).

MNF transform was performed using the ENVI software package (ITT 2010). Based on joint inspection of scree plot information, percentage of the variance explained, and visual assessment of image spatial coherency, 15 MNF bands were selected to be used in subsequent analyses. These MNF 15 bands explain 71.48% of the variance.

The other dimensionality-reduction method employed was independent component (IC) analysis. Independent component analysis is a blind-source separation tool that does not require any prior information to compute. It utilizes a non-Gaussian assumption of independent sources and is able to separate and reveal features in hyperspectral data. One of the advantages of IC analysis is that it can distinguish features that may only occupy a small portion of the pixels within an image (Hyvärinen, Karhunen and Oja 2004).

IC analysis was performed on the Hyperion image and 7 bands were chosen for subsequent analyses; these 7 bands explain 65.4% of the variance. The same criteria used in MNF band selection were also used for selecting the IC bands to propagate to further analysis steps.

4.2.3 Vegetation indices

Various vegetation indices were calculated (Table 2). Vegetation indices are dimensionless, radiometric measures that indicate relative abundance and activity of green vegetation (Jensen 1996). Vegetation indices often can provide unique biophysical information that is not necessarily apparent from radiance or reflectance values. Various applications of vegetation indices include estimation of leaf area index (Suits 1973), percentage of cover (Carlson and Ripley 1997), chlorophyll content (Tucker 1979), among others. For the purpose of this study, a suite of hyperspectral vegetation indices was generated using ENVI software based on the good Hyperion bands that were available after spectral subsetting.

4.3 Geomorphometric and biophysical variable pre-processing

The geomorphometric variables were all produced from a LiDAR-derived digital terrain model (DTM). These variables included elevation, slope, aspect, profile curvature, plan curvature (Zevenbergen and Thorne 1987), and topographic wetness index (TWI) (Beven and Kirkby 1979). In addition, a Euclidean distance to river variable was calculated. The LiDAR data used were acquired 3 June, 2011. LiDAR data processing was done in collaboration with Dr. Jason Tullis, University of Arkansas. The processing was performed using LASTools within ArcMap 10.2.

Index	Formula	Citation
Normalized Difference Vegetation Index (NDVI)	$\mathrm{NDVI} = \frac{\mathrm{NIR} - \mathrm{RED}}{\mathrm{NIR} + \mathrm{RED}}$	(Rouse 1974)
Atmospherically Resistant Vegetation Index (ARVI)	$\mathrm{ARVI} = \frac{\mathrm{NIR} - 2\mathrm{RED} - \mathrm{BLUE}}{\mathrm{NIR} + 2\mathrm{RED} - \mathrm{BLUE}}$	(Kaufman and Tanré 1996)
Red Edge NDVI ($NDVI_{705}$)	$\mathrm{NDVI}_{705} = \frac{750 - 705}{750 + 705}$	(Gitelson and Merzlyak 1996)
Modified Red-Edge Simple Ratio (mSR_{705})	$\mathrm{mSR}_{705} = \frac{750 - 445}{705 - 445}$	(Datt 1999)
Modified Red-Edge NDVI ($mNDVI_{705}$)	$\mathrm{mNDVI}_{705} \frac{750 - 705}{750 + 705 - 2(445)}$	(Datt 1999)
Vogelmann Red-Edge Index (VOG1)	$\mathrm{VOG1} \frac{740}{720}$	(Vogelmann, Rock and Moss 1993)
Photochemical Reflectance Index (PRI)	$\mathrm{PRI} = \frac{531 - 570}{531 + 570}$	(Gamon, Penuelas and Field 1992)
Structure Insensitive Pigment Index (SIPI)	$\mathrm{SIPI} = \frac{800 - 445}{800 - 680}$	(Penuelas, Baret and Filella 1995)
Red Green Ratio Index (RG ratio index)	$\mathrm{RG\ Ratio} = \frac{\mu\ \mathrm{Red\ Bands}}{\mu\ \mathrm{Green\ Bands}}$	(Gamon and Surfus 1999)

Table 2 - Hyperspectral vegetation indices computed.

The basic workflow for this processing consisted of the following steps. 1) Identify noise points and exclude these points from processing. 2) Select last return points 3) Classify the last return points using the following parameters step: 5; spike: 1; stdev: 10; and offset: 0.05”. The classification consisted of 3 classes, unassigned, ground or noise. 4) Apply a ground filter using the following parameters step:1, isolated:2. 5) Filter points to achieve ground points and then triangulate these points without thinning, and 6) Generate a digital elevation model (DEM) that is used in conjunction with an aerial photograph to find LiDAR points that were incorrectly classified. A final DTM was then produced from these points (personal communication, J. Tullis, 2014).

In addition to the LiDAR data covering the study area, the same data-processing flow was performed on other LiDAR data sets in the vicinity of the study area that were spatially coincident with known survey points from National Geodetic Survey (NGS). These NGS points were used in a pseudo accuracy assessment. A survey-grade GPS/GNSS receiver was not available to perform a DTM accuracy evaluation within the study area itself, so in order to determine the validity of the LiDAR processing, these NGS-surveyed control points were used as a proxy. Average vertical difference between the 8 NGS elevations and the spatially-corresponding LiDAR-derived elevations was 0.48 meters.

The soil variables used were the percentage values of the sand, silt and clay at each site, as well as the texture of the soil as classified by the United States Department of Agriculture (Figure. 6) . Soil raster layers for the entire site were computed using a kernel interpolation. A Gaussian kernel function, polynomial order of 1, and a ridge parameter of 25 were used. The USDA texture classification was generated using the QGIS program (QGIS 2014).

Aboveground biomass (AGB) for the forest was remotely estimated in an associated study in this same study area using some of the same nonparametric-modeling methods as those employed in the current study (Filippi et al. 2014, Güneralp et al. 2014b). Using the dbh collected during the 2010 fieldwork, *in situ* aboveground biomass at each field site was determined using allometric equations. Allometric equations use a set of psychical parameters, such as dbh, and/or height, to approximate the biomass of certain tree species or functional groups of species. When possible, species-specific allometric equations were used, and when these were not available functional group equations were used.

Once the AGB associated with each field site was determined based on *in situ* data, those *in situ* AGB values were used for nonparametric regression model development. Three different nonparametric algorithms were used to perform multiple dataset-combination trials, similar to the procedure used for the current study. The nonparametric algorithms investigated for remote-sensing AGB estimation were Cubist (Huang and Townshend 2003) multivariate adaptive regression splines (MARS), and stochastic gradient boosting (SGB). MARS and SGB are discussed in Section 4.4. Cubist is a regression tree model that produces rule-based results. Cubist served as the baseline algorithm against which the remote-sensing AGB estimates from the other two algorithms were compared.

Across the multispectral and hyperspectral image-driven trials conducted (Filippi et al. 2014, Güneralp et al. 2014b), MARS produced the most accurate AGB estimates using 30-m Landsat 5 image data. Specifically, MARS Experiment 2, where multispectral image bands and image-derived variables (such as vegetation indices) were used as input, yielded a root mean squared error (RMSE) of 29.2 tonnes/ha AGB and a coefficient of determination (R^2) = 0.94 (Filippi et al. 2014, Güneralp et al. 2014b). The remote sensing-estimated

AGB for the study area from this particular experiment (Figure 7) were used as an input variable for Chinese tallow-detection model development.

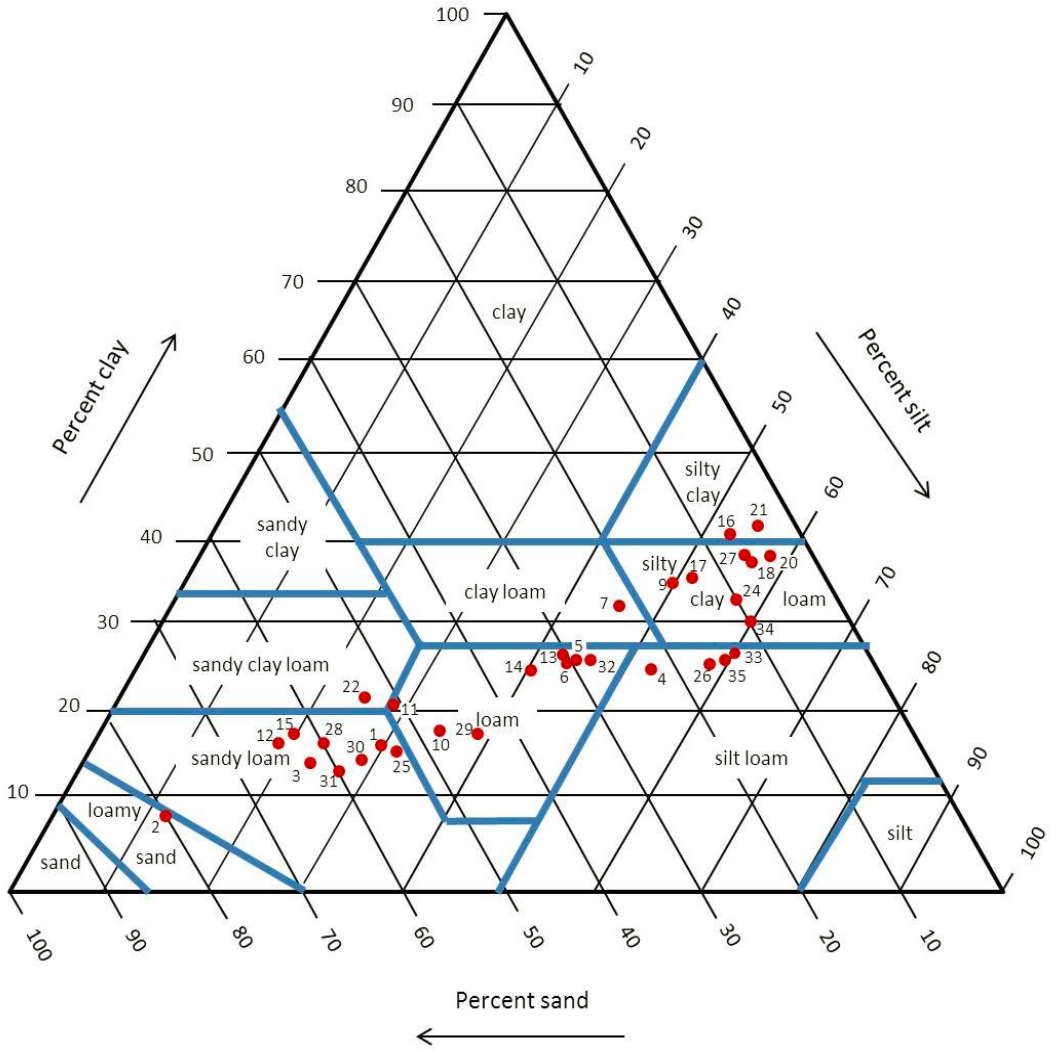

Figure 6 - USDA soil classifications with study site soil classification locations (red circles) (Nyikos 2011).

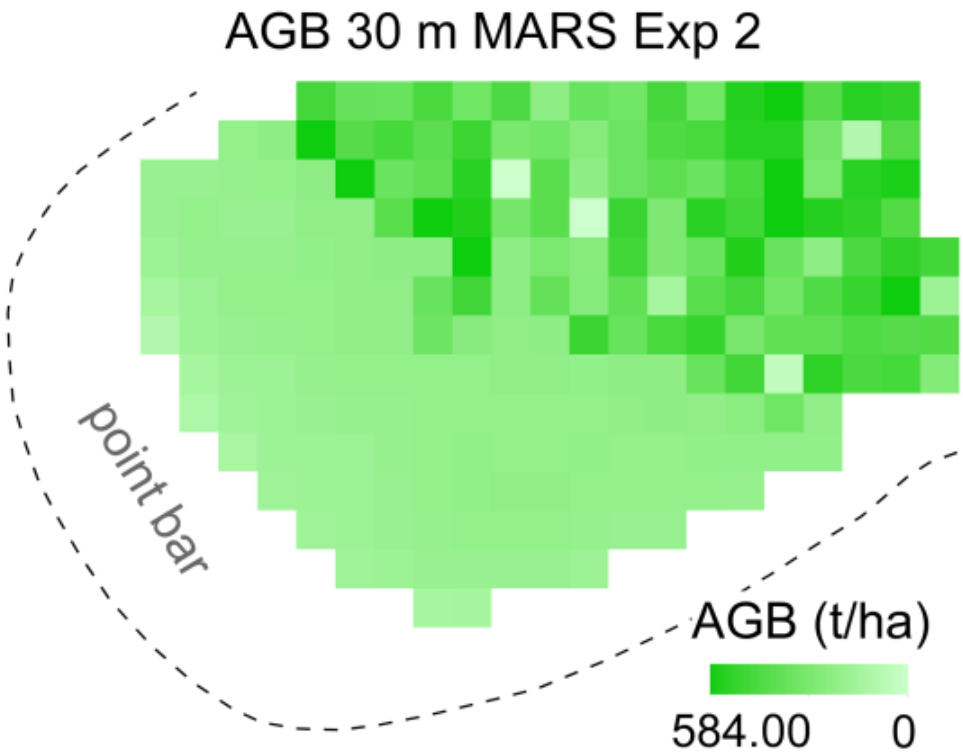

Figure 7 - Aboveground biomass (AGB) estimates derived using MARS. RMSE = 29.2 tonnes/ha AGB and (R^2) = 0.94 (Güneralp et al. 2014b).

4.4 Nonparametric modeling algorithms

Three different nonparametric algorithms were used to detect/classify Chinese tallow in the floodplain forest on the meander bend: Random Forests (RF) (Breiman 2001), MARS (Friedman 1991), and SGB (Friedman 2002). These three algorithms were implemented using the Salford SPM software package (SalfordSystems 2014). Nonparametric methods may be appropriate for detecting tallow, given non-linearities in most floodplain/riparian forest systems (Güneralp et al. 2014b). Each of these algorithms yields hard

classification results, as well as classification probability values for each individual pixel in the image. These classification probability values can be used as a proxy for fractional abundance of material/class of interest (e.g., Chinese tallow) in a given pixel. Thus, these probability/pseudo-fractional-abundance values can be compared with spectral unmixing results, such as those obtained via mixture-tuned matched filtering (Mellor et al. 2013). Although some vegetation remote-sensing classification studies seek to detect/classify all species in an area, this was not the focus of this study, as it likely would not be feasible given the relatively coarse-spatial resolution of the image and the lack of homogeneity of the species within the image pixels.

4.4.1 Random forests

Random forests (RF) is a data-mining technique that expands upon the more basic classification tree method (Breiman et al. 1984). RF is able to fit many trees to a data set instead of just one tree. The predictions from all of these trees are combined into one final result. When each tree is built it selects a sample from the data known as the bootstrap sample. These are the samples used for training of the model. The remaining samples are referred to as out-of-bag observations and effectively become the testing sample for the model. These out-of-bag results are effectively a cross validated accuracy estimates. This is important because the other methods that are compared to RF use cross validation and therefore there can be a direct comparison between methods.

One of the benefits of RF is that when measuring variable importance RF takes a misclassification rate from the out-of-bag observations. Values of a specific variable are randomly taken form the out-of-bag data and passed to the tree to get a new prediction. The difference between the original misclassification rate and the modified rate divided by the standard error represents the importance of that particular variable.

For this study the following parameters were used within the software to produce the various trial results: number of trees: 500; predictors at each node: 6; progress report frequency: 10; proximal cases: automatically chosen; bootstrap sample size: automatically chosen; and parent node minimum cases: 2. These parameters were set based on the recommendation from the software producer (SalfordSystems 2014) and trial-and-error experimentation. Whereas RF is much more robust technique compared with simpler classification and regression trees (Breiman et al. 1984, Cutler et al. 2007), there are newer nonparametric methods that were anticipated to perform better. RF was thus used as a machine-learning baseline for this study, as various other previous ecological studies have already found success with RF (Cutler et al. 2007, Latifi, Nothdurft and Koch 2010, Prasad, Iverson and Liaw 2006).

4.4.2 Multivariate adaptive regression splines

MARS is an adaptive non-linear regression technique that utilizes piecewise basis-functions (Friedman 1991). These basis functions define

relationships among response variables and the predictors. The basis functions are set up in pairs using a knot that defines an inflection point. This knot is a value within the range of the given predictor. This allows for there to be different slopes within different parts of the range of the regression. There is also the possibility of using more than one knot which is in essence the use of more than 2 basis functions.

A forward stepwise procedure is used to choose the placement of the knots. A step is defined when the model selects the placement of the knot and the particular basis functions that are used. When the maximum model size is reached a backward pruning takes place to remove basis functions that do not contribute to the model are removed. A pseudo version of cross-validation is performed to evaluate the best model with the best predictive fit.

One of the benefits of MARS is that variable interactions can also be fitted into the model allowing for a more dynamic interaction between predictor variables. Although MARS is inherently a regression technique, it can be used in this study as a classification model because of the binary nature of the species modeling. A version of MARS utilizing logistic binary regression can be used to classify a Boolean variable such as tallow/non-tallow. This binary regression does not change the MARS model but rather evaluates the result probabilities and then uses a cutoff of 0.5 to classify the results into a 0 or 1 (tallow or non-tallow). The set parameter values used for the MARS dataset-combination trials in this study are as follows: max basis functions: 15; maximum interactions

between predictors: 2; and min observations between knots: 1. These parameter values were chosen after systematically testing of the effect of a range of values for each individual parameter, while holding the values for the other parameters constant. The set of values for the MARS parameters, noted above, yielded the most accurate results.

The model was tested using 10-fold cross validation. Cross validation is a testing technique that allows for the entire sample data set to be segregated into 10 parts or folds and then run 10 times using 9 of the folds as training and the final fold as testing. At each of the 10 folds, a different fold is used for testing. This allows for all the data to be used in both the training and testing phase of the modeling process. The MARS model was bootstrapped 10 times so that 10 models were built, each of them using 10-fold cross validation. The best model was chosen from these 10 models. The reason 10 was chosen as the number of models to build was because beyond ten there were not significant changes among the results.

MARS has been successfully employed to solve a variety of ecological problems. These include: modeling species distributions (Leathwick, Elith and Hastie 2006), predictive habitat modeling (Moisen and Frescino 2002, Muñoz and Felicísimo 2004, Prasad et al. 2006), characterization of soil properties (Shepherd and Walsh 2002), invasive species mapping (Stohlgren et al. 2010) and aboveground biomass estimation (Filippi et al. 2014, Güneralp et al. 2014b).

4.4.3 Stochastic gradient boosting

Stochastic gradient boosting (Friedman 2002) is a variant of more basic regression tree models. SGB makes many small classifications using many smaller regression tree models. The gradient of the loss function from one of these small trees is used as a pseudo-residual to better train the subsequent tree. A random subset of the data is used during each iteration of the model. This contributes to a gradual improvement of the model over time (Friedman 2002).

Some of the advantages of SGB which set it apart from other models are that is stochastic and as such there should not be a need to pre-select variables. SGB should be able to determine which variables are of use in the final model development. It is resistant to outliers because it focuses more on points closer to the correct classification. SGB uses only a fraction of the training data making it resistant to over-fitting.

SGB has been used in few ecological applications thus far. It has been used to model aboveground biomass (Filippi et al. 2014, Güneralp et al. 2014b), predict tree presence and basal area (Moisen et al. 2006), and to measure the distribution of freshwater fish (Elith, Leathwick and Hastie 2008). SGB is a robust nonparametric model, and it is thus a very useful algorithm to which the other models investigated in this study can be compared.

A total of 2000 trees were built for each trial and at each fold of the 10-fold cross-validation process. As with MARS, cross validation was used to obtain

the best model. In addition, the process was bootstrapped 10 times in order to yield the best possible model. The number of minimum node training cases was 4, and the maximum nodes per tree was 6. The regression loss criterion used was a blend of least squares and least absolute deviation (Huber 2011).

4.4.4 Modeling trials

In order to assess the importance of certain types of input variables and their effects on Chinese tallow classification accuracy, 19 different dataset-combination trials were conducted. These trials involved different groups of predictor variables, and the efficacies of various combinations of input variable groups were evaluated. Across the three nonparametric modeling algorithms considered, the same input variable groupings and combinations were used for the 19 trials conducted per algorithm (Table 3).

Data type	Details	Trial
Hyperion image bands (wavelength range 426.82 – 2335.01 nm)	115 bands: Bands 9-12, 101, 134, 164, 183, 187-197, 199-203, 205-206, 219	1-4,17,19
Minimum noise fraction images (MNF)	15 MNF images (71.48% of the variance explained)	5-8,17,19
Independent component images (IC)	7 IC images (65.4% of the variance explained)	9-12,17,19
Vegetation indices	NDVI, ARVI, $NDVI_{705, m}SR_{705}$, $mNDVI_{705}$, VOGL, PRI, SIPI, RG ratio index	13-16,17,19
Geomorphometric variables	Elevation, slope, aspect, plan curvature, profile curvature, TWI, Euclidean distance to water	2,4,6,8,10,12,14,16,18, 19
Biophysical characteristics (Soils, AGB)	Soil texture and percentages (sand,silt,clay), aboveground biomass	3,4,7,8,11,12,15,16,18, 19

Table 3 - Predictor variables used in the classification trials across all of the algorithms. MNF and IC bands were derived from the hyperion image. Geomorphometric variables were derived from a LiDAR-based DTM (LiDAR point-cloud source: Texas Water Development Board).

4.5 Spectral analysis

Multiple endmember-based spectral analyses were performed including spectral angle mapper (SAM) (Yuhas, Goetz and Boardman 1992), spectral feature fitting (SFF) (Clark and Swayze 1995), and mixture-tuned matched filtering (MTMF) (Boardman 1998). SAM generates an angular match value, whereas MTMF produces fractional abundances that can potentially be compared with the nonparametric model-derived probability values. These analyses were performed on both field-derived endmembers and an image-derived endmember for Chinese tallow.

The basic workflow for all of these analyses can be seen in Figure 8. The first step to attain the image reflectance has already been detailed. The second step is to a spectral data reduction using an MNF. This time more MNF images were used to obtain endmembers than the images used in the nonparametric models. These 33 MNF bands contained 79.85% of the variance. More MNF bands were used in order to better determine the image derived spectral endmember for Chinese tallow.

The pixel purity index (PPI) finds the most spectrally-pure pixels in the image. To accomplish this, *n*-Dimensional scatter plots are projected onto a random unit vector. Typically, this is performed for thousands of iterations in order to find the most extreme pixels as possible. For this study, 75,000 PPI-computation iterations were performed. Once PPI computation has terminated, the *n*-Dimensonal viewer was used to determine the endmember(s) that

correspond to Chinese tallow based on the field results. 34 endmembers were produced from the 33 MNF images. PPI assumes there is one spectrally-pure pixel in the image for each of the endmembers. This is an issue in this research as the image is very complex and different trees and types of vegetation are intermixed and make for very little spectrally pure pixels.

Spectral feature fitting is a more basic spectral analysis that compares the fit between image spectra and reference spectra. It uses a least-squares technique. SFF uses continuum removal to match the image and reference spectra. The output is a scale image for the reference spectra that indicates the strength of the fit.

Spectral angle mapper is a spectral classification technique that uses the n-Dimensional angle to match pixels to reference spectra. The angle is treated as a vector in a space with dimensionality equal to the number of bands, in this case 33, the smaller the angle the closer the match to the spectra. For the SAM classification, the threshold was set at the default of 0.1 radians. The output from this is a rule image that contains an angular value for each pixel that indicates the degree of match with the endmember spectrum, where smaller angular values denote a closer match.

Mixture-tuned matched filtering is based on matched filtering and adds an infeasibility image to the results. Matched filtering uses a partial unmixing to suppress the response of unknown background materials and accentuate the response of the known endmember (Boardman 1998). It is a good technique to

use when only trying to match one endmember as in the case of this research. The infeasibility image used in MTMF is used in combination with the matched filtering score to create a set of rule images for each endmember. The value is the relative degree of the match between the reference spectra and approximate sub-pixel abundance. These relative abundance values will compare best with the previous nonparametric model probability values.

Field spectra were taken during the first portion of field collection in 2010. These spectra were applied to the same techniques as the image derived spectra, but did not yield good results. The spectra exhibited higher reflectance values than the image reflectance values and also did not cover as much of the spectrum and therefore were not able to compare favorably with the image.

Field spectra were taken during the first portion of field collection in 2010. These spectra were applied to the same techniques as the image derived spectra, but did not yield good results. The spectra exhibited higher reflectance values than the image reflectance values and also did not cover as much of the spectrum and therefore were not able to compare favorably with the image.

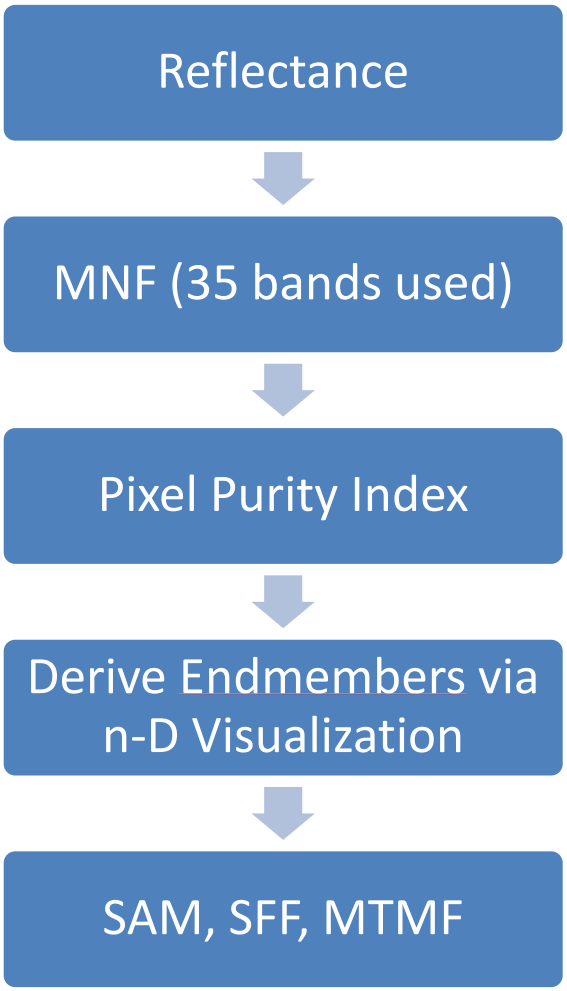

Figure 8 - Spectral analysis workflow. All steps were completed within ENVI.

4.6 Spatial statistical analysis

A Getis-Ord Gi* hot-spot analysis was performed on the best tallow-prediction results from each of the three nonparametric classification methods to quantitatively characterize the spatial distribution of Chinese tallow trees. Before performing the hot-spot analysis, a spatial autocorrelation test was run using a range of distance thresholds at 30-m increments to determine the ideal distance band to utilize in the hot-spot analysis. The SGB- and RF-based hot-spot analyses both were performed using a distance threshold of 30 m, whereas the MARS-based hot-spot analysis was performed using a threshold of 60 m. This hot-spot analysis is of particular benefit because it can identify areas where there are statistically-significant clusters of high or low probabilities of tallow presence. These areas may exhibit certain conditions that are more (less) ideal for tallow growth than other areas.

4.7 Nonparametric model statistical comparison

The results of the models with the highest accuracy from each of the three nonparametric models were compared to one another using the McNemar statistical test. The McNemar test is a statistical measure used when comparing multiple binary classifications, and it determines whether they have a similar marginal distribution between the two classifications (Foody and Mathur 2004, Duro, Franklin and Dubé 2012). The McNemar test is similar to a paired sample t-test; however it is conceptually the testing of two different properties of a

repeated measure dichotomous variable. It is used to compare pretest-posttest designs or analyzing comparisons between methods, as is the case in this study. It is a good test to use when the same phenomenon is being analyzed twice. In the case of this study, it is the binary true/false response from the three different nonparametric models evaluated.

In McNemar's test and a Pearson's chi-square test, the Yates correction factor is often applied. This correction factor is used to prevent overestimation. Often the Yates correction factor tends to overcorrect, but in the case of this study's data it is applicable. Use of the Yates correction factor is recommended if a small data set is being analyzed, and if the data set is binary in nature. SPSS (IBM 2013), the software used to generate the McNemar statistics does not give the option to exclude the correction factor and applies it automatically (IBM 2013); in the case of the testing data used in this study, this is acceptable.

All of the algorithms compared utilized cross-validation as a validation technique. It may be of concern that the same testing data was not being used in each of the algorithms. Using cross-validation, it was ensured that each of the points in the small-sized sample was used once for testing. Therefore, the same points were used as testing points for each of the algorithms. Statistical comparisons between the algorithms are therefore efficacious. Cross-validation testing results like these have been used in similar types of classification comparisons (Brenning 2009, Torresan et al. 2014).

5. RESULTS

5.1 Field observations

Observations from fieldwork conducted in 2010 and 2014 reveal that, relative to other areas on the meander bend, there is a higher density of tallow trees present in/along the transitional zone between the more mature forest and the smaller tree/shrub zone closer to the point bar. The chute that cuts through half of the meander-bend study area runs directly through and parallel with this transition zone. The availability of water and the ability of tallow to tolerate flooding (Butterfield et al. 2004) may at least partially explain this pattern. In addition, this transition zone represents an area of river meander migration-induced disturbance, and is part of an intermediate light regime and it is thus prone to Chinese tallow colonization.

Moving southwest away from the chute towards the point-bar, there are also relatively high numbers of Chinese tallow trees. This may be due to more access to sunlight because of the presence of shorter vegetation and more open canopy. This portion of the meander bend has historically been the most disturbed and flooded, including a flooding event in 1994. Because of the more frequent flooding in the southwestern part of the meander bend, vegetation tends to be younger there and more diverse, relative to other parts of the meander bend. Therefore, this portion of the study area is more susceptible to tallow invasion. Areas very close to the point-bar that do not have very much vegetation exhibited very little instances of tallow growth. This may be due to the

soil characteristics in this the newest part of the meander bend, and this area experiences the highest flood frequency (at least once a year) (personal communication, Stuart Marcus, 2015) compared with other areas of the meander bend, which allows for little to no plant establishment. Further from the river, where the more established, more mature forest, which has been stable for the most part for the past 60 years, is located, there are very few instances of tallow (i.e., no more than five (5) instances in a given field plot). The fact that there are instances of Chinese tallow in these more mature-forest areas though may serve as indicator of its ability to colonize to some degree over a wide extent of the study area.

5.2 Nonparametric model results

All model results reported (Tables 4-6) are based on the OOB or cross-validation testing of each model. Use of OOB and cross-validation ensures that every sample is used at least once for testing. All 70 samples are used to produce result statistics and confusion matrices that contain test results (not training results).

A variety of different metrics were used to assess model accuracy for each trial, for each nonparametric-modeling algorithm. Average log-likelihood is not as strong a metric as some of the other metrics but is still useful. It is a logarithmic version of the likelihood function, which emphasizes the probability interpretations of a model's prediction (the lower the value, the more accurate

the model). Misclass rate is simply the percentages of test results that were classified incorrectly and therefore will mirror the final classification results produced. Although this seems redundant, it may provide a different context in which to evaluate a model. Receiver operating characteristic (ROC) (Equation 1), or area under the curve, is one of the more commonly-used metrics to assess model accuracy, particularly in binary classification models. The ROC is a plotted using the following equation:

$$\frac{\frac{\text{True Positives}}{\text{Positives}}}{\frac{\text{False Positives}}{\text{Positives}}}$$

Equation 1: Receiver operating characteristic (ROC)

ROC is used in this study, along with the overall classification accuracy, to choose the best model or models generated by each of the algorithms. These are compared against each other, as well as against other results from the other classification methods.

Random Forest Results						
	Predictor variables used	Average LogLikelihood	Misclass Rate	ROC (area under curve)	Lift	% Correct (0.5 Threshold)
Trial 1	Bands	0.515	0.228	0.837	1.3	77.14
Trial 2	Bands, Geomorph	0.5	0.228	**0.851**	1.5	77.14
Trial 3	Bands, AGB, Soils	0.505	0.228	0.85	1.5	77.14
Trial 4	Bands, Geomorph, AGB, Soils	0.5	**0.2**	0.845	1.5	**80**
Trial 5	MNF	0.54	**0.2**	0.799	**1.8**	**80**
Trial 6	MNF, Geomorph	0.544	0.242	0.807	1.3	75.71
Trial 7	MNF, AGB, Soils	0.547	0.228	0.802	1.3	77.14
Trial 8	MNF, Geomorph, AGB, Soils	0.554	0.271	0.801	1.3	72.85
Trial 9	IC	0.544	0.287	0.802	**1.8**	71.42
Trial 10	IC, Geomorph	0.574	0.285	0.792	1.3	71.42
Trial 11	IC, AGB, Soils	0.548	0.271	0.788	**1.8**	72.85
Trial 12	IC, Geomorph, AGB, Soils	0.555	0.342	0.795	**1.8**	65.71
Trial 13	Veg Indices	0.69	0.371	0.68	1.5	62.85
Trial 14	Veg Indices, Geomorph	0.602	0.342	0.75	1.5	65.71
Trial 15	Veg Indices, AGB, Soils	0.625	0.342	0.734	**1.8**	65.71
Trial 16	Veg Indices, Geomorph, AGB, Soils	0.603	0.285	0.748	1.5	71.42
Trial 17	Bands, MNF, IC, and Veg Indices	0.482	0.228	0.847	1.5	77.14
Trial 18	AGB, Soils, and Geomorph	0.611	0.3	0.722	1.5	70
Trial 19	All variables	**0.486**	**0.2**	0.849	1.5	**80**

Table 4 - Statistical results from the random forest nonparametric model trials. Trials 1-19 are all listed including the variables used in the associated trial. Numbers in bold indicate the best result for the corresponding statistical metric.

MARS Results							
	Predictor variables used	Number of basis functions	Average LogLikelihood	Misclass Rate Overall (raw)	ROC (area under curve)	Lift	% Correct (0.5 Threshold)
Trial 1	Bands	10	0.153	0.1	0.898	1.4	88.57
Trial 2	Bands, Geomorph	11	0.298	0.085	0.927	1.8	90
Trial 3	Bands, AGB, Soils	10	0.177	0.1	0.906	1.4	84.29
Trial 4	Bands, Geomorph, AGB, and Soils	9	0.268	0.085	0.963	1.8	87.14
Trial 5	MNF	13	0.31	0.142	0.919	2	**92.85**
Trial 6	MNF, Geomorph	12	0.205	0.1	0.979	1.8	85.71
Trial 7	MNF, AGB, Soils	13	0.244	0.114	0.909	1.6	87.14
Trial 8	MNF, Geomorph, AGB, and Soils	12	0.171	0.1	0.957	1.6	91.43
Trial 9	IC	14	0.224	0.114	0.955	1.9	87.14
Trial 10	IC, Geomorph	9	0.185	0.1	0.928	1.5	81.43
Trial 11	IC, AGB, Soils	15	0.336	0.114	0.914	**2.1**	**92.85**
Trial 12	IC, Geomorph, AGB, and Soils	12	0.162	**0.071**	0.962	1.8	75.71
Trial 13	Veg Indices	14	0.592	0.257	0.826	1.8	77.14
Trial 14	Veg Indices, Geomorph	8	0.259	0.128	0.935	1.8	82.86
Trial 15	Veg Indices, AGB, Soils	7	0.412	0.157	0.879	1.6	78.57
Trial 16	Veg Indices, Geomorph, AGB, and Soils	13	0.372	0.228	0.819	1.3	82.86
Trial 17	Bands, MNF, IC, and Veg Indices	13	0.144	**0.071**	**0.99**	1.8	88.57
Trial 18	AGB, Soils, and Geomorph	10	0.256	0.171	0.916	2	85.71
Trial 19	All variables	15	**0.143**	**0.071**	**0.99**	1.8	88.57

Table 5 - Statistical results from the MARS nonparametric model trials. Trials 1-19 are all listed including the variables used in the associated trial. Numbers in bold indicate the best result for the corresponding statistical metric.

SGB Results							
	Predictor variables used	Optimal number of trees	Average LogLikelihood	Misclass rate	ROC (area under curve)	Lift	% Correct (0.5 threshold)
Trial 1	Bands	331	0.377	0.142	0.889	1.46	91.42
Trial 2	Bands, Geomorph	332	0.368	**0.114**	0.889	1.46	91.42
Trial 3	Bands, AGB, Soils	332	0.383	0.157	0.882	1.46	91.42
Trial 4	Bands, Geomorph, AGB, Soils	330	**0.374**	**0.114**	0.891	1.46	91.42
Trial 5	MNF	284	0.534	0.214	0.793	1.53	87.14
Trial 6	MNF, Geomorph	311	0.484	228	0.862	1.53	88.57
Trial 7	MNF, AGB, Soils	161	0.575	0.271	0.774	1.79	90
Trial 8	MNF, Geomorph, AGB, Soils	299	0.529	0.2	0.815	1.53	90
Trial 9	IC	484	0.505	0.2	0.837	1.42	88.57
Trial 10	IC, Geomorph	413	0.522	0.271	0.827	**1.89**	**92.85**
Trial 11	IC, AGB, Soils	132	0.575	0.228	0.752	1.84	82.85
Trial 12	IC, Geomorph, AGB, Soils	192	0.628	0.257	0.702	**1.89**	87.14
Trial 13	Veg Indices	82	0.599	0.271	0.76	1.42	72.85
Trial 14	Veg Indices, Geomorph	124	0.682	0.314	0.636	0.76	85.71
Trial 15	Veg Indices, AGB, Soils	168	0.643	0.285	0.703	1.08	84.28
Trial 16	Veg Indices, Geomorph, AGB, Soils	131	0.648	0.242	0.625	0.52	84.28
Trial 17	Bands, MNF, IC, and Veg Indices	358	0.435	0.157	0.875	1.42	**92.85**
Trial 18	AGB, Soils, and Geomorph	107	0.673	0.257	0.613	0.78	81.42
Trial 19	All	572	0.389	0.171	**0.9**	1.46	**92.85**

Table 6 - Statistical results from the SGB nonparametric model trials. Trials 1-19 are all listed including the variables used in the associated trial. Numbers in bold indicate the best result for the corresponding statistical metric.

Lift indicates the effectiveness of the model as a ratio of the testing results obtained. The higher the number the more likely the model is to be a strong, unbiased model. The final metric used is simply the overall classification accuracy of the experiment. This is the accuracy of the testing data withheld in each fold or out-of-bag that was used for testing. For a hard, binary classification, a threshold value of 0.5 was used to determine whether a data point is classified as tallow or non-tallow. This threshold was used because the software manual (SalfordSystems 2014) recommended initially using this value as the threshold, and other studies have used the same threshold in a similar type of analysis (Mellor et al. 2013).

In addition, a few other important characteristics of models from certain algorithms are included in these tabular results. For instance, the optimal number of basis functions is included in the MARS results table (Table 5). The number of basis functions does not necessarily represent the strength of the model, but rather may provide more detail on the model and its complexity. More basis functions indicate more use of different predictor variables within the model. The SGB results (Table 6) include a similar metric that indicates the ideal number of trees. 1000 trees were built at each fold of the cross-validation model, but 1000 trees were not always the optimal number of trees to build. The number of trees may be indicative of the strength of each model to continue to improve on the previously built tree before it. More trees indicate that the model was able to sift through more predictors to find the optimal combinations of

predictors. Models with fewer trees built may have had less or not very strong predictors (Friedman 2002).

There was not one dataset-trial across all three algorithms that performed the best overall, meaning there was not one dataset combination used with the three classification algorithms that was best across all of the statistical metrics, but there were some that performed well with respect to multiple metrics. Regarding overall classification accuracy, trial 19 for both RF and SGB yielded the highest overall accuracy for each algorithm (80% and 92.85% overall accuracy, respectively), except that RF trials 4 and 5 also returned 80% overall accuracy (tied with RF trial 19). SGB trials 10 and 17 also generated an overall accuracy of 92.85%. MARS also had two models (trials 5 and 11) that yielded overall accuracies of 92.85%.

ROC values did not always match the overall classification accuracies. The best RF ROC was with trial 2, with a value of 0.851. MARS had the best overall ROC values, with trials 17 and 19 achieving ROC values of 0.99. SGB had one trial with a ROC value of 0.9 (trial 19). SGB trial 19 was the only trial that had both the highest ROC and overall percent correct. Given that SGB iteratively corrects the model using pseudo-residuals and chooses new predictors, it is not surprising that the model that included all predictors was the best, most accurate model.

Comparing the confusion matrices for best trial results for the three nonparametric algorithms (Tables 7-9), it is clear that that both MARS and SGB

performed better than RF. Average overall classification accuracies across all trials showed that MARS (average percentage correct = 88.5%) was slightly more accurate than SGB (average percentage correct = 87.73%), and both were more accurate than RF (average percentage correct = 73.22%).

Given the confusion matrices for the best models (Tables 7-9), selected using overall percentage correct as the primary criterion and then ROC as a second criterion, there is little difference between the MARS and SGB results, aside from MARS having one more false positive than SGB. RF also has a higher number of false positives compared to false negatives.

Classification	Non-tallow	Tallow	Producer Accuracy(%)	
Non-tallow	25	5	83.3	
Tallow	9	31	77.5	
User Accuracy (%)	73.5	86.1		
			Overall Accuracy	80

Table 7 - RF trial 19 confusion matrix

Classification	Non-tallow	Tallow	Producer Accuracy(%)	
Non-tallow	28	2	93.3	
Tallow	3	37	92.5	
User Accuracy(%)	90.3	94.8		
			Overall Accuracy	92.8

Table 8 - MARS trial 5 confusion matrix

Classification	Non-tallow	Tallow	Producer Accuracy(%)	
Non-tallow	27	3	90	
Tallow	2	38	95	
User Accuracy(%)	93.1	92.6		
			Overall Accuracy	92.8

Table 9 - SGB trial 19 confusion matrix

The three best models were applied to all of the data in the study area to create maps showing both predicted binary results as well as predicted probability results. These maps show what are final predictions for where tallow was at the time the image was taken as well as the probability of tallow being in that area. The models were built with one instance of tallow indicating the presence of tallow, therefore some of these areas may in reality not include much tallow but according to the model built there should at least be one instance of tallow in the represented area.

The RF models were shown to be the weakest of the models with only an 80% accuracy, but that is still a relatively high score and overall the general trend of the data in the predicted maps seems to mirror the field and observational data. In general there is not tallow near the point bar and deeper in the more established forest. There are a few patches that were not predicted to contain tallow in more of the transitional zone that there tended to be more tallow, but these area did have field sites that did not contain tallow so that may be a factor in these predictions (Figure 9).

While there are some pixels in the probability map that are closer to the threshold value of 0.5 the majority of pixels are closer to either 0 or 1 and indicate that according to the model there is a high confidence that these locations are predicted accurately (Figure 10). There is a similar pattern in this map as all the other maps and that is the further away from the transition zone where the largest concentration of tallow is the less tallow it is predicting. This could be a function of the model but this general trend was also observed in the field data. However if this model is to be used to predict tallow on a larger scale the models built in this study may not be ideal because they may represent this special environment and not the entire landscape in general.

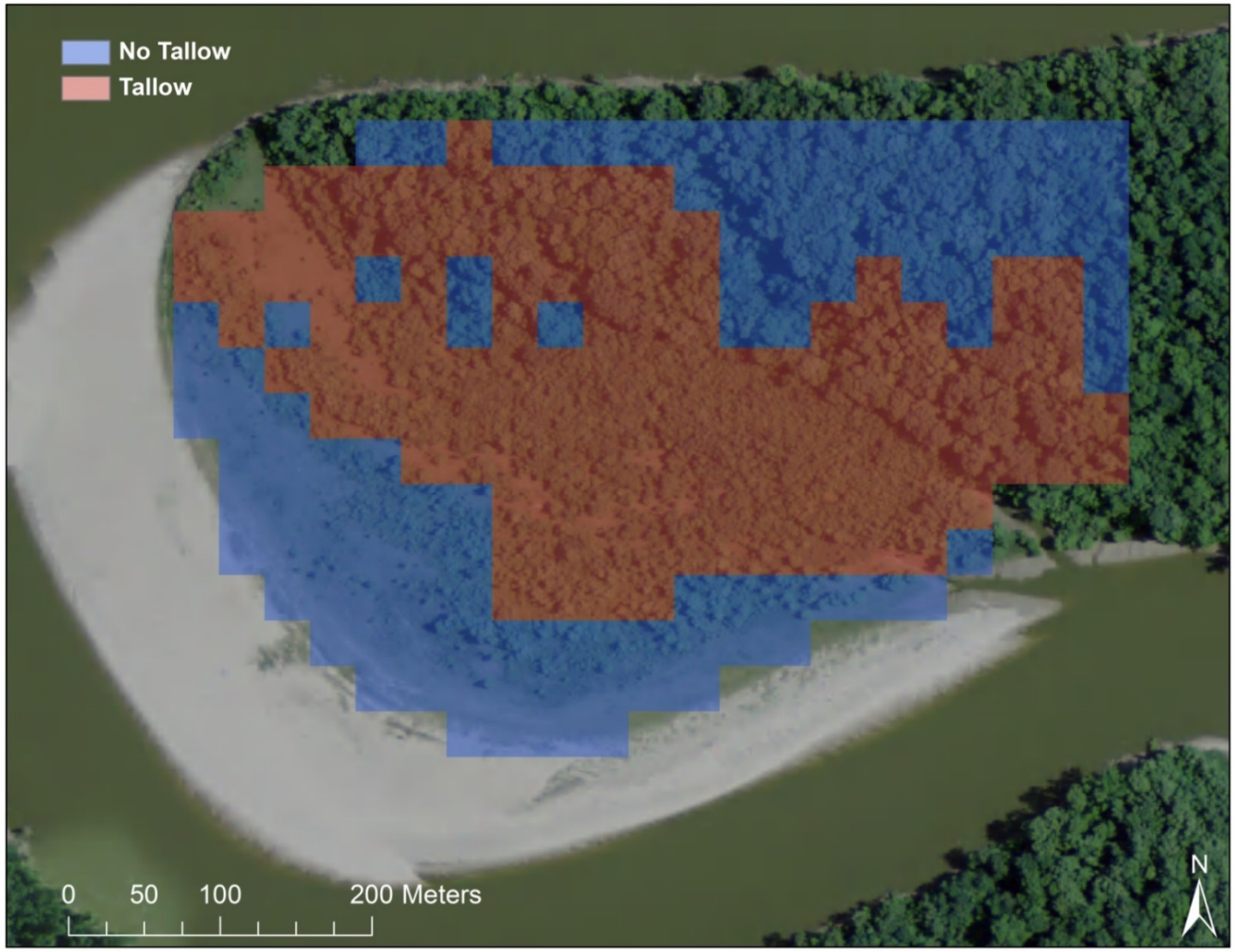

Figure 9 - RF experiment 19 projected binary model results for the entire study area. Background imagery taken from 2008 (National Agriculture imagery project)

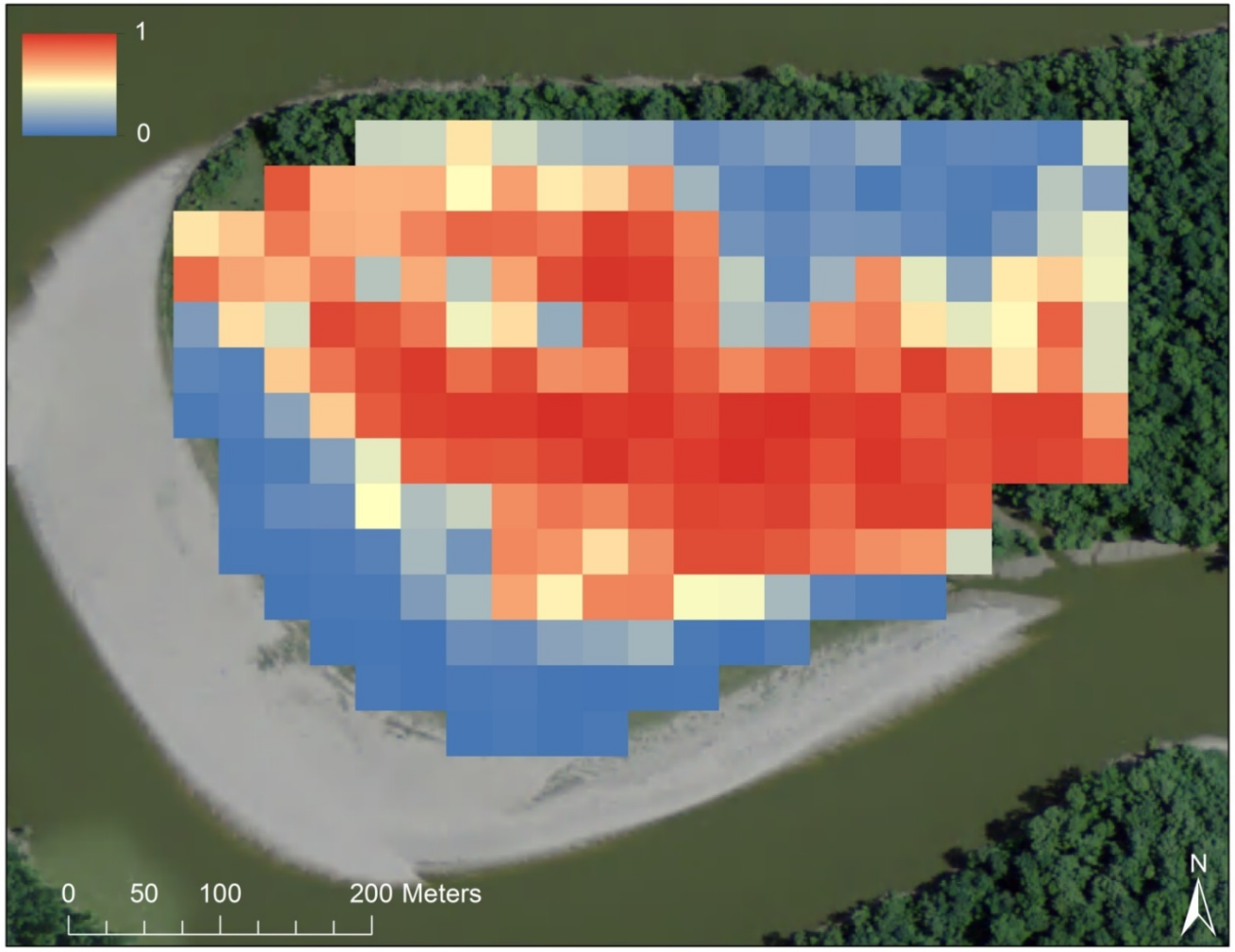

Figure 10 - RF experiment 19 projected probability model results for the entire study area. Background imagery taken from 2008 (National Agriculture imagery project)

The MARS binary prediction map (Figure 11) differs somewhat from the RF map. In the MARS classification image, there are more predicted tallow pixels in the more mature forest areas. This is probably due to the fact that a few field plots in the more mature forest did have at least one instance of tallow. The model is taking these instances of few tallow trees and equating them to tallow presence, these instances of sites with a small number of tallow trees are interpreted by the models in terms of tallow presence/absence, which appears to lead to tallow overestimation. Particularly in the more mature forest, there is very likely an overestimation of the number of pixels that should be classified as tallow. This could at least partially be an artifact of the smaller number of *in situ* field plots in those areas.

MARS probabilities differ from those derived from RF and SGB. The probability values from MARS trial 5 (Figure 12) do not seem as extreme as those from the other two algorithms. There are many more cells that are close to the 0.5 threshold than the other two algorithms. This could mean could mean that it was more difficult for MARS to generate a binary result based on the training data, or it could mean that MARS is a better soft classifier, in a sense, and is more precise than the other models.

RF and SGB are both essentially regression tree models, whereas MARS uses more basic linear regression techniques. This may be an important distinction in future studies when choosing a modeling method. It is important to note that MARS is using a binary classification technique and cannot classify multiple

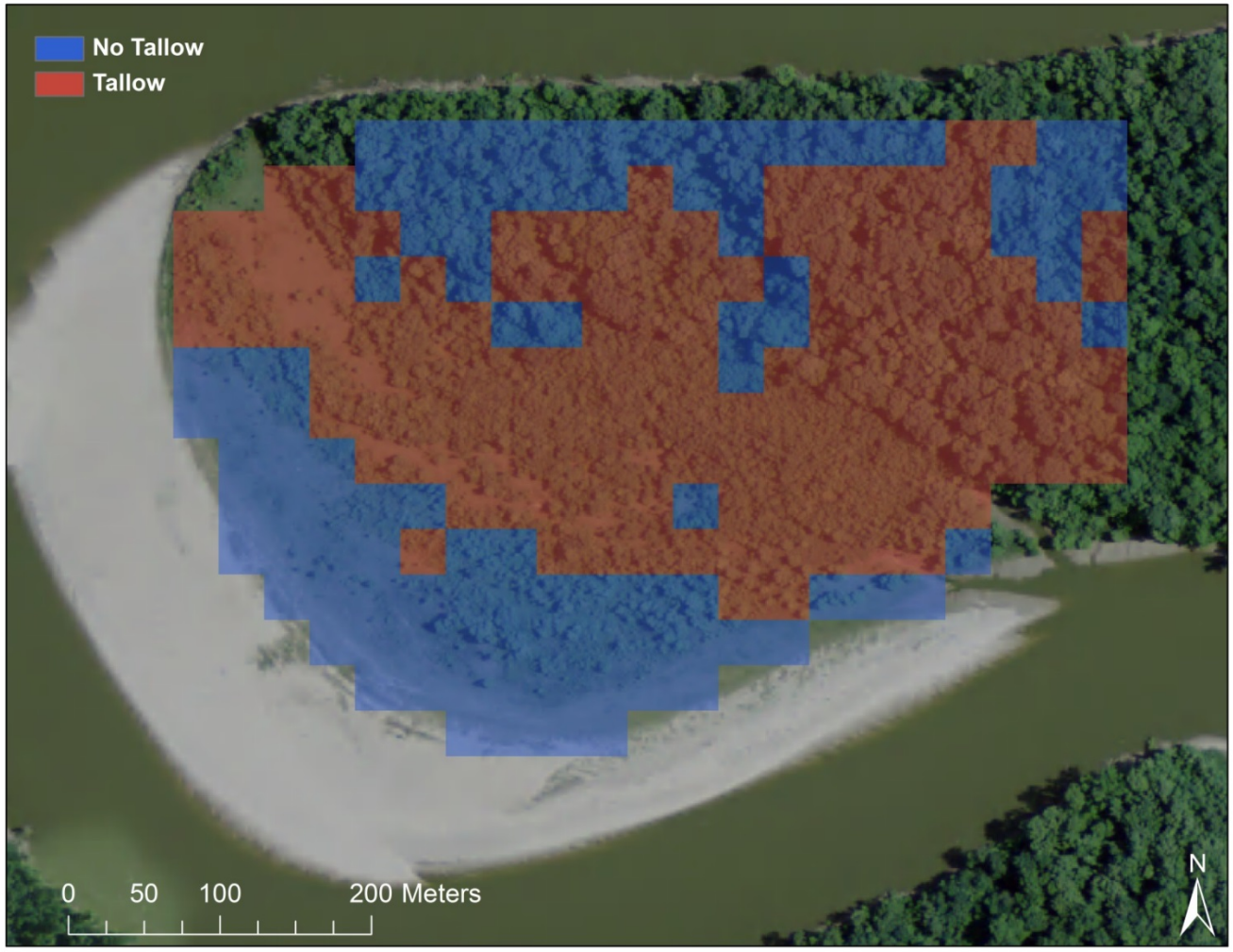

Figure 11 - MARS experiment 5 projected binary model results for the entire study area. Background imagery taken from 2008 (National Agriculture Imagery Project)

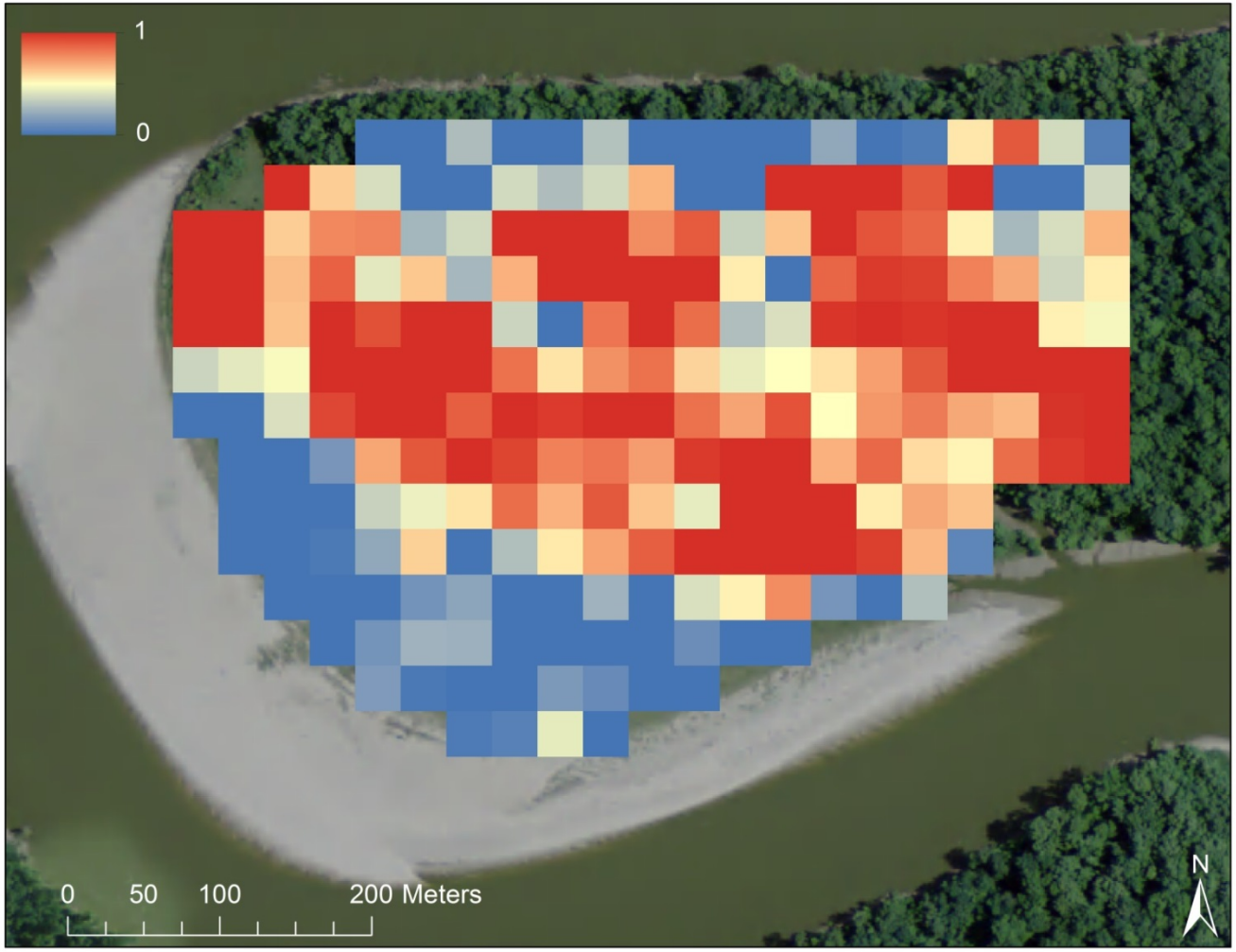

Figure 12– MARS experiment 5 projected probability model results for the entire study area. Background imagery taken from 2008 (National Agriculture imagery project)

classes. Regardless, or perhaps because of this, MARS produced some of the best Chinese tallow classifications in this study.

The SGB binary map (Figure 13) resembles the RF map more closely than the MARS map, but statsitcally is more accurate than RF (Tables 7-9). On the eastern side of the study area where there were not as many sample points there is possibly an overestimation of tallow occurrence. This area is mature forest and field observations show that this area should have less tallow than others, but the model may overpredict due to the lack of training data in that area. SGB predicts more tallow in that area than the other two algorithms.

SGB also does not predict as many tallow-free pixels in the center of the study area as the other algorithms.The SGB map indicates the model was very rigid in regards to the training data. The two pixels in the middle of the map that were predicted as non-tallow were both non-tallow training areas, but the model did not grow these areas at all. The model tended to indicate that the area around these pixels was closer to the area where there is a lot of tallow growing and predicted those as tallow pixels.

Similar to RF, the probability map (Figure 14) is more biased toward either tallow or non-tallow, there are not many pixels near the threshold value. This may suggest that with these data, the regression models tended to have more bimoda probability values in this type of binary classification. In comparing these two regression tree techniques SGB is more comprhensive algorithm in its use of all prediction variables and its iterative nature makes it stronger than RF.

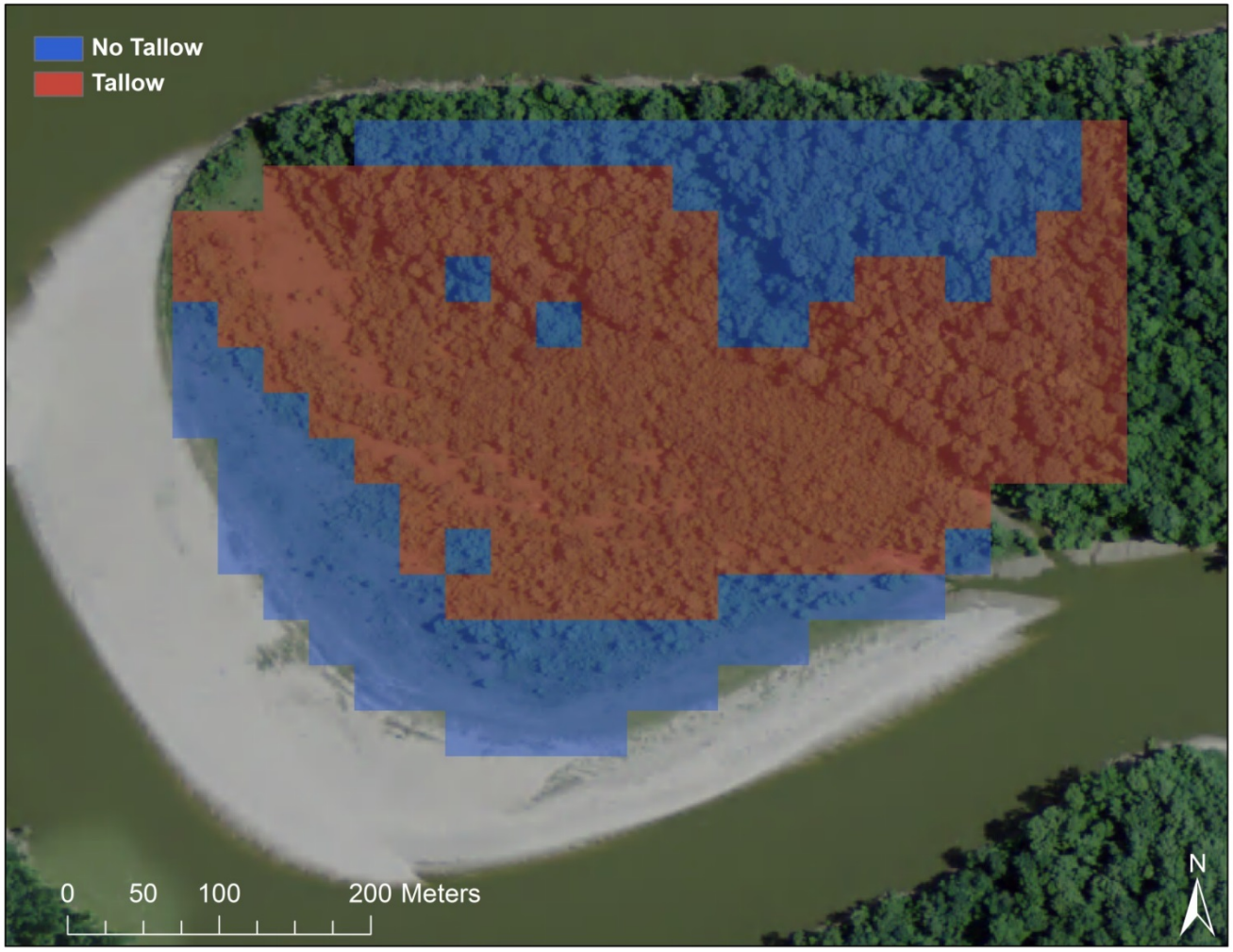

Figure 13 - SGB experiment 19 projected binary model results for the entire study area. Background imagery taken from 2008 (National Agriculture imagery project)

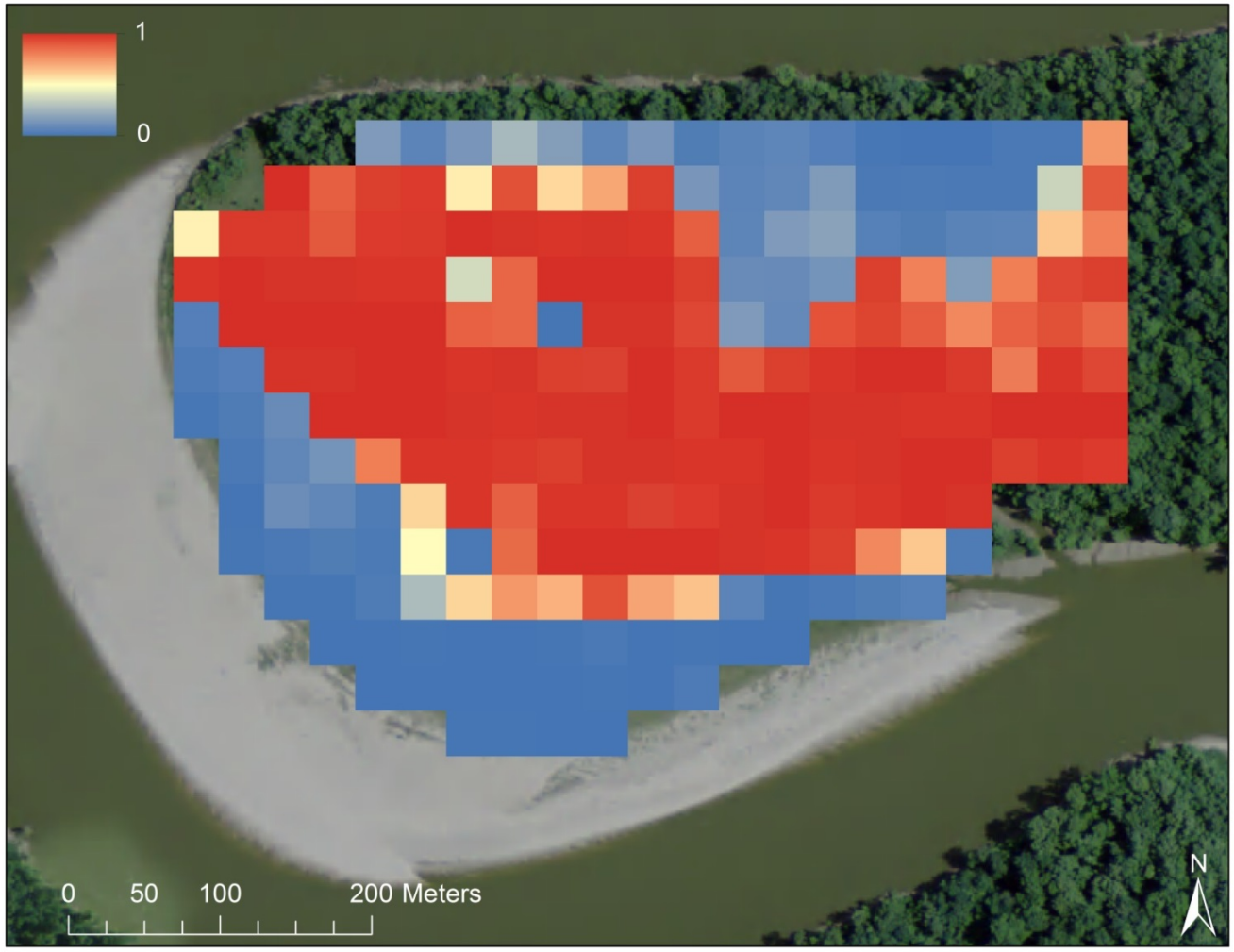

Figure 14 – SGB 19 projected probability model results for the entire study area. Background imagery taken from 2008 (National Agriculture imagery project)

SGB has the ability to identify the most imporant predictor variables and use those variables in model construction whereas RF needs more user input. The MARS and SGB statistical results (i.e overall accuracy) are idnetical and there is no statistical significant difference between them.

MARS trial 5 and SGB trial 19 have identical overall statistical accuracies. However, there are some differences when analyzing their predicted results for the entire study area (Figure 15). The map shows where there are areas of disagreement between the MARS and SGB predictions.

The area that seems to have the most disagreement between the models is again in the denser, mature forest portion of the study area. This may be traced back to the possible over-prediction of tallow pixels in the MARS experiment. Although MARS is not as biased/extreme in its probability map there does seem to be an over-prediction of tallow sites in the area. Based on the statistical results and without further testing sites in the more established part of the forest it is difficult to make an assumption that there is or is not tallow there. This makes it difficult to say which model outperformed the other but it can be stated that if a more complex classification is needed then SGB is the modeling algorithm of choice in that situation.

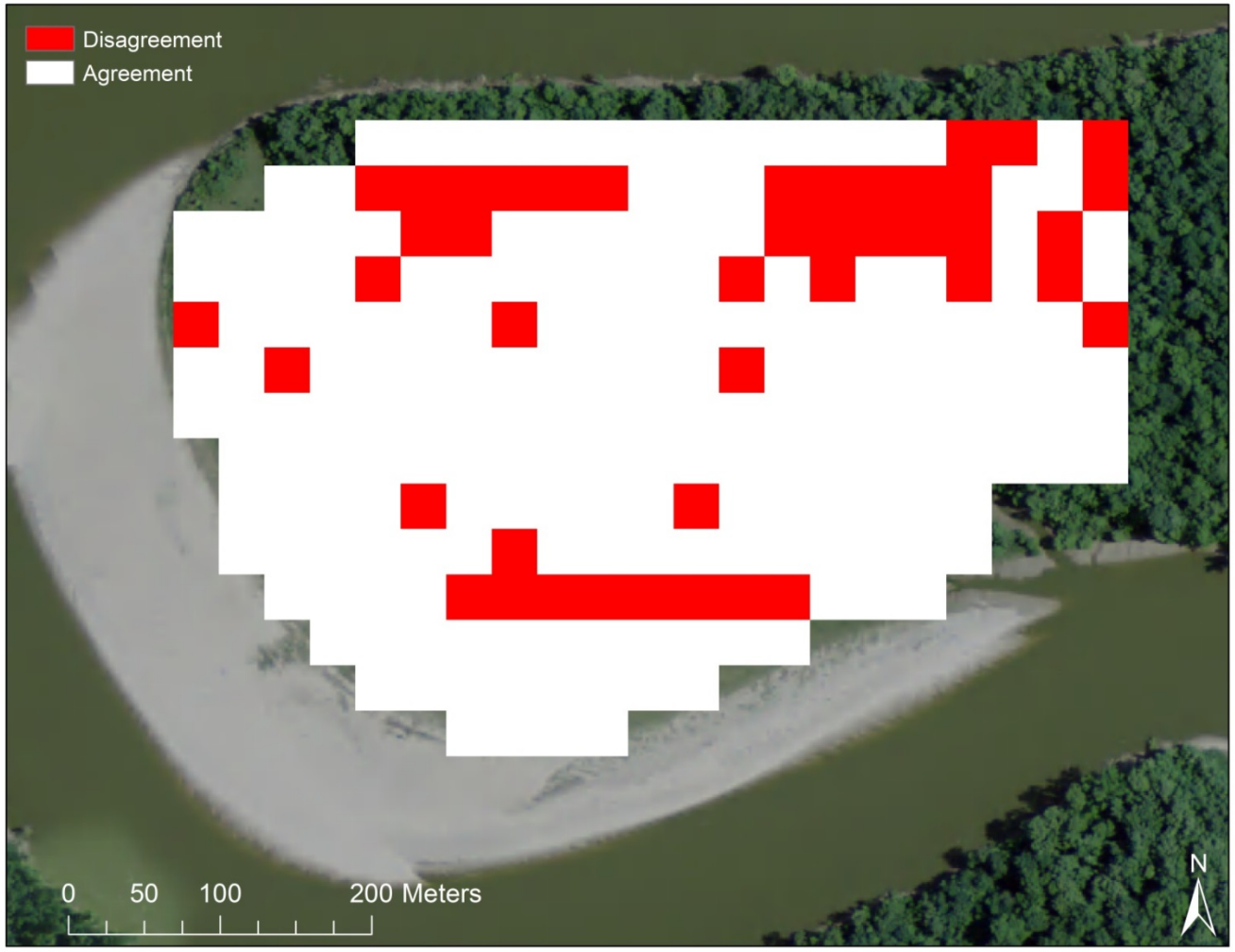

Figure 15 – A map comparing the agreement between the ideal predicted values for MARS (experiment 5), and SGB (experiment 19). These were the best experiments among the non-parametric models

Low tallow analysis (zero tallow sites included)			
	RF	MARS	SGB
< 5% occurrence correct (n=3)	90.91%	72.73%	81.82%
< 20% occurrence correct (n=9)	76.47%	58.82%	58.82%
< 50% occurrence correct (n=15)	60.87%	43.48%	43.48%

Table 10 - Areas of low tallow correctly classified by nonparametric algorithms (zero tallow sites included)

Low tallow analysis (zero tallow sites not included)			
	RF	MARS	SGB
< 5% occurrence correct (n=11)	66.67%	33.33%	33.33%
< 20% occurrence correct (n=17)	55.56%	33.33%	22.22%
< 50% occurrence correct (n=23)	40.00%	20.00%	13.33%

Table 11 - Areas of low tallow correctly classified by nonparametric algorithms (zero tallow sites not included)

5.3 Spectral analysis results

The spectral analysis results, in general, tend to under-predict the presence of Chinese tallow. In most of the results utilizing spectral feature fitting (Figure 16), spectral angle mapper (SAM) (Figure 17) and mixture-tuned matched filtering (MTMF) (Figure 18) the area where the image-derived spectra are located are classified accurately, but under-prediction is prevalent in the rest of the study area, with the exception of the SAM results.

SFF uses a least-squares technique to diagnose the fit between the reference and image spectra. It utilizes continuum removal in order to scale the images to each other. The resulting output is a combined “fit” map which combines the scale and RMS image output from the model (Figure 16). The higher the value the better the fit or match to the reference spectra.

The results from SFF indicate that where there is a more dominant presence of tallow along the chute there is a high fit. This also is where the image derived spectra are located so it is not surprising to see a high fit there. There is a good prediction closer to the point bar where there is less tallow and less vegetation in general, but further inland of the point bar the results are very spotty and variable and do not seem to follow the *in-situ* data as well as the nonparametric modeling algorithm results.

Because SFF it does not contain fractional abundance values it is difficult to compare it directly to the nonparametric algorithms, but it is a good baseline method to compare the other spectral analysis methods against.

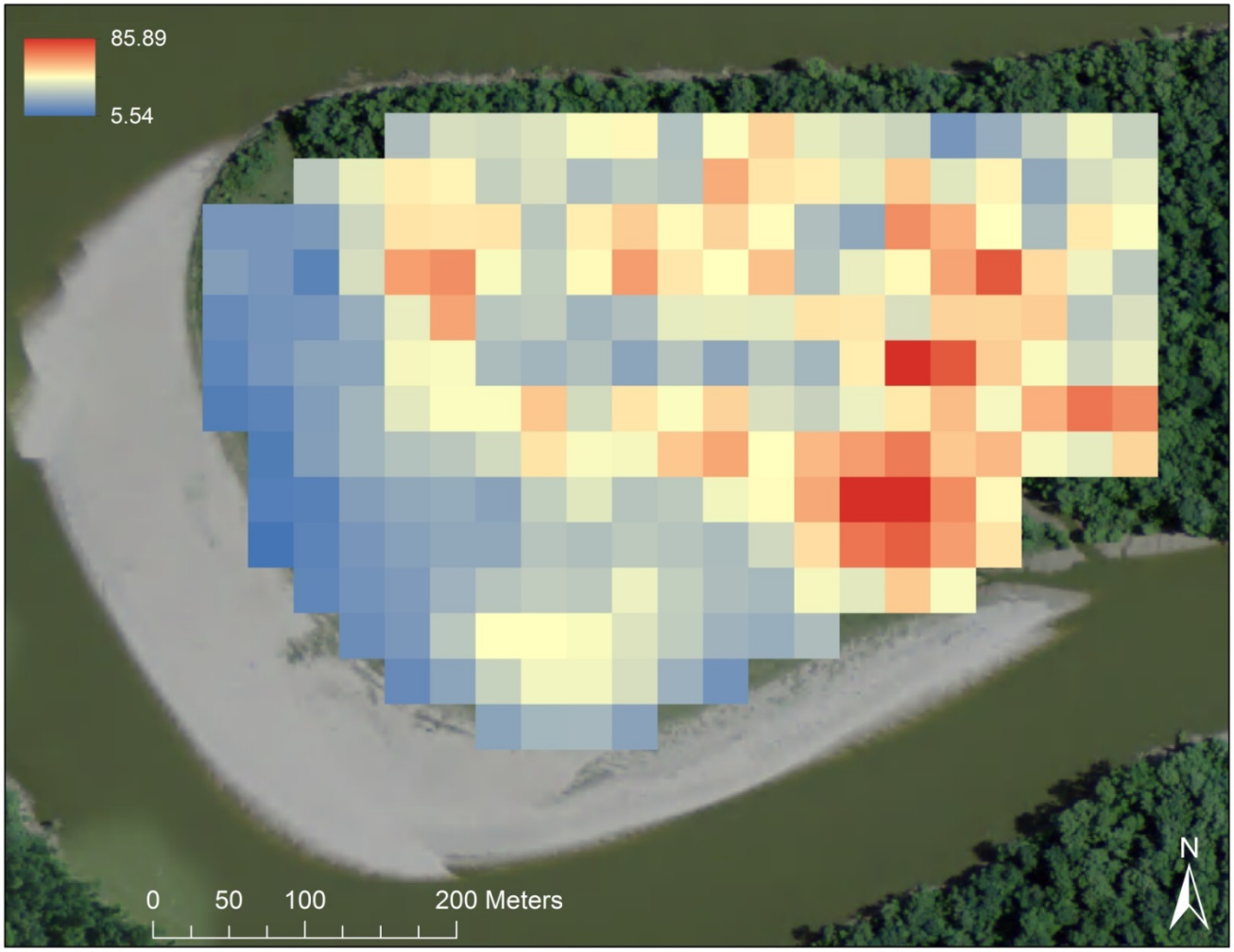

Figure 16 - This SFF fit map combines both the scale and RMS result images from SFF to show the best fit between the reference and image spectra. Higher values represent a better fit.

The SAM results (Figure 17) are different from the two other spectra analysis methods in that it appears to be over-predicting tallow, but due to the results of SAM being the size of the angle between the reference and target spectra small changes in the angular value may indicate bigger changes in the actual classification. In a SAM classification the lower the angular value the better the match.

The SAM results indicate a strong association between the reference and target spectra in the same location as the other classifications (Figure 17). Along the chute there is a strong relationship. Looking at the SAM results it looks like almost anywhere that there is significant amount of vegetation on the point bar it is predicting tallow, but this may be a little misleading due to the small changes in the angular values of each pixel. The lighter red pixels may really be insinuating a weak relationship between the two spectra. This map is useful in that it is most likely realistically showing where tallow could be present but the amount of tallow at each location is not represented very well with this type of a classification. It is too generalized to really make an assumption about whether there is tallow at a location or not, and in reality there are not very many limiting factors in regards to tallow growth besides extreme temperatures and over-saturation.

SFF as well as SAM both generate outputs that make them difficult to compare to each other and to compare with the nonparametric models, nevertheless the visual patterns can still be compared. The amount of *in situ*

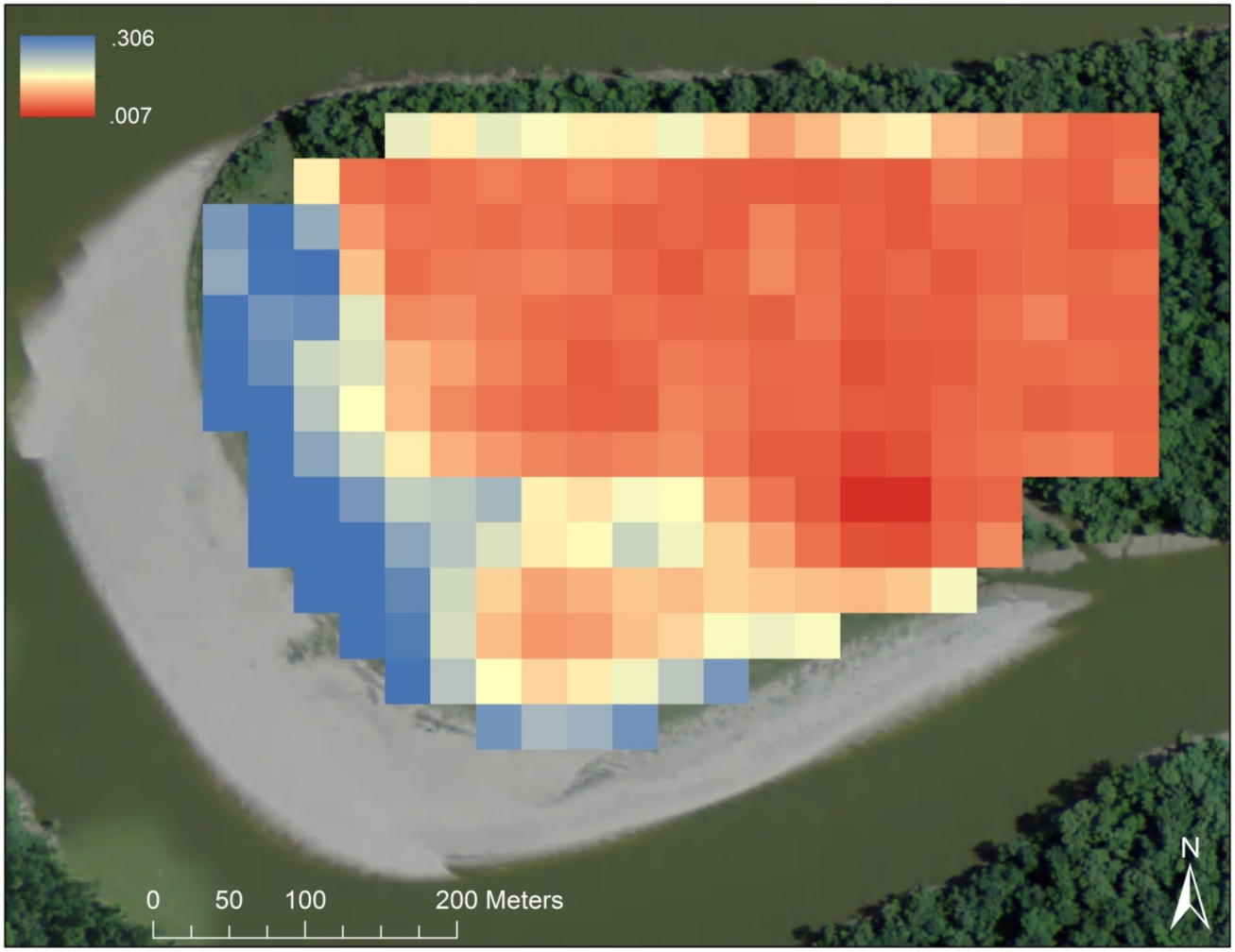

Figure 17 – SAM results, values are angular values between the endmember spectrum vector and each pixel vector in the image.

data collected where the largest amount of tallow is has led to most of the models predicting well there and overall the general trend in the SAM and other models is in line with the *in situ* data.

The MTMF result (Figure 18) is composed of a fractional abundance value for each pixel. This abundance value makes it possible to compare this method to the other nonparametric methods. The resulting classification image shows the results in a two-tailed pattern. There are very few pixels that show a moderate result but rather there are many values close to 0 or close to 1.

The pattern seen in other results is continued in this image with the area near the chute and where the tallow end-member was derived exhibiting a high probability of tallow occurrence. While many of the other classifications generalized the whole area as a probable location for tallow growth MTMF predicts no tallow in locations that most certainly contain tallow. MTMF exhibited the worst results of all of the methods.

5.4 Method comparisons

MTMF yields fractional abundances, so these were compared with nonparametric model-derived probabilities. The best model result (MARS trial 5) and the MTMF results were compared using a map algebra local subtraction operation (Figure 19). Areas that are most likely incorrect in the MTMF image are not in agreement with the MARS image. Specifically, there is an under-prediction of tallow in the MTMF image which is creating a large difference.

While these areas contain less tallow than right along the transitional zone near the chute, they still contain rather large numbers of tallow trees.

In this instance, the spectral-analysis results less accurate and do not seem to follow the patterns observed in the field. This does not mean that the nonparametric modeling algorithms are the best choice nor does it imply they are completely correct, but observation of the results does seem to imply that they outperform in this study.

In summary, the best results are those achieved using SGB and MARS. These techniques were able to better parse through the testing data and determine areas in the study area that are more amenable to tallow growth. The spectral results were not as conclusive and that is likely due to a number of factors including spatial resolution, lack of true tallow spectra, tallow as an understory species, and pixels containing a large variety of species that are difficult to spectrally un-mix.

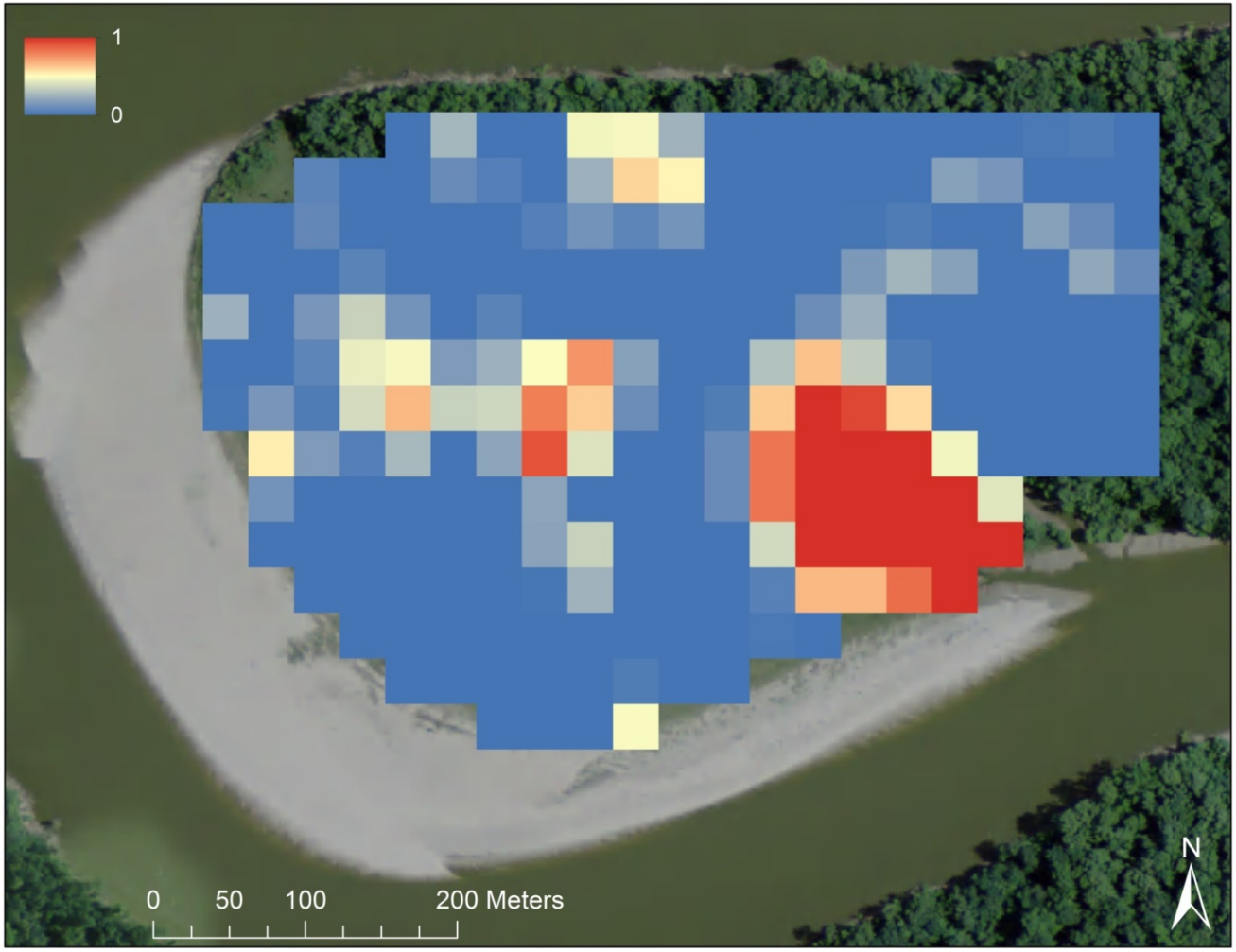

Figure 18 - MTMF results image, values are fractional abundances of tallow. There is a distinct separation between high abundance and low abundance areas and possible overtraining localized around areas with high amounts of tallow.

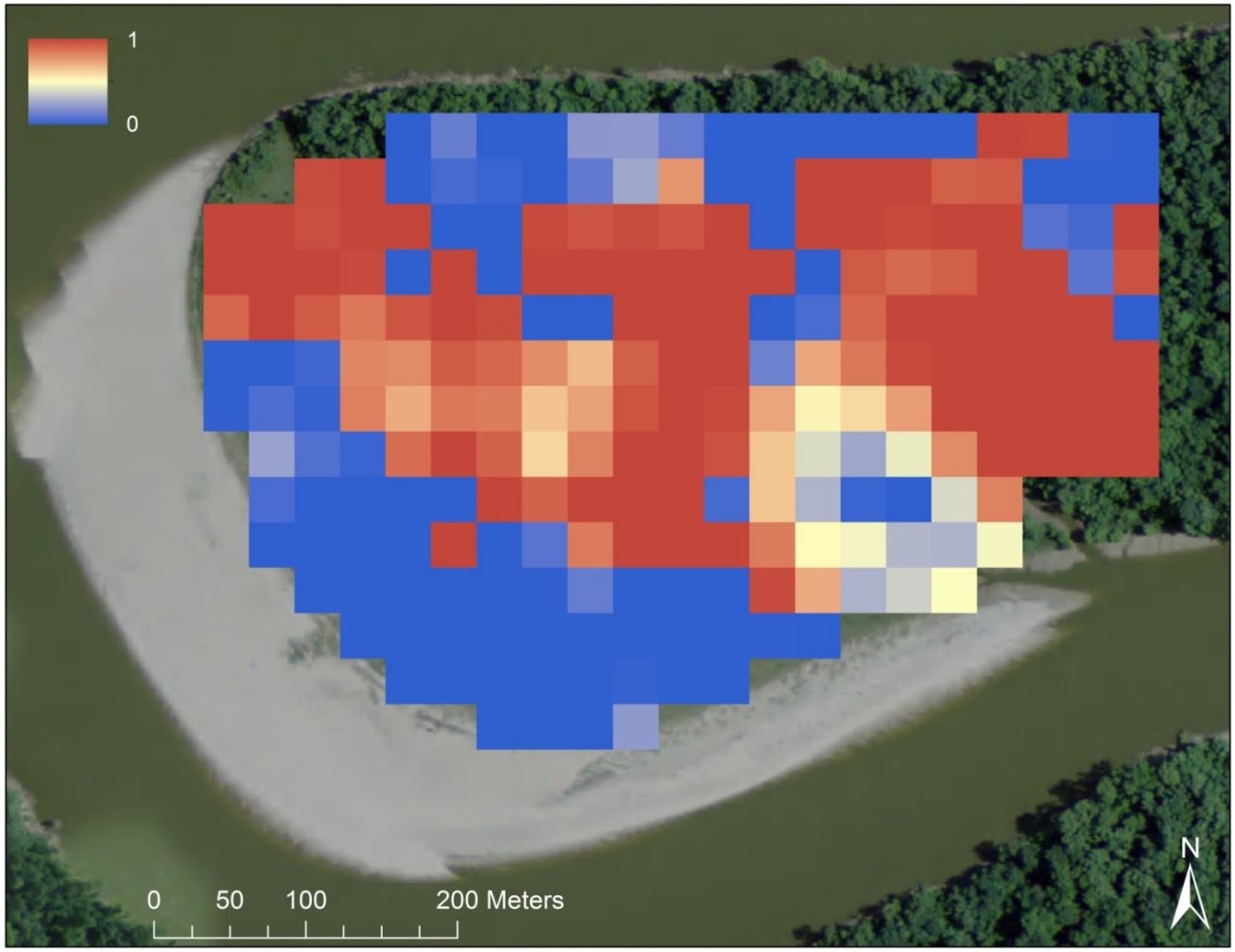

Figure 19 – The difference between the percent abundance values of the MTMF and MARS results. Areas in blue are in more agreement than those areas in red.

5.5 Spatial analysis

A Gettis-Ord GI hot-spot analysis was produced for the probability values from each of the best models generated by the three modeling methods (Figures 20-22). Hot spot analysis is beneficial because it identifies statistically significant spatial clusters of high values (hot spots) and low values (cold spots). Clustered areas of tallow should be highlighted in red colors representing high z-values, and blue cold spots should representing clusters of areas where tallow growth is not very likely.

In the three hot-spot maps (Figures 20-22), the colors represent z values. These z values represent the number of standard deviations away from the mean these values are. High and low z values are outliers and thus represent a clustering of values that are unlike the mean and thus unlike the majority of the pixels. Z-scores above 2.6 are significant at the 99^{th} percentile; z-scores in between 1.96 and 2.6 are significant at the 95^{th} percentile.

These hot-spot maps reinforce what is visible in the field and from a majority of the models. The area that entails the highest number of Chinese tallow trees is along the transitional zone/boundary between mature forest and younger forest. In addition, the chute cut that provides a water-delivery mechanism to this area may contribute to more tallow growth and spread.

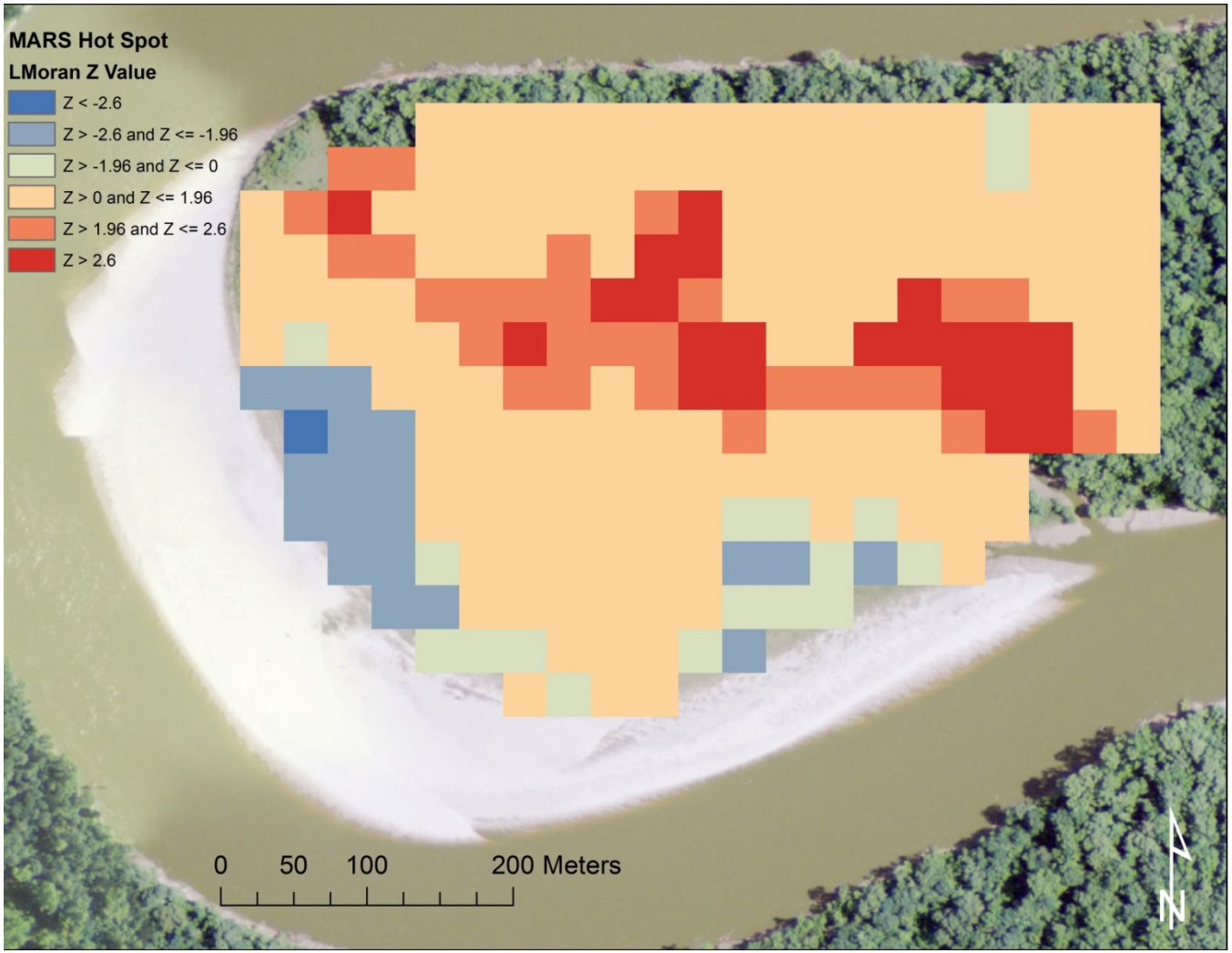

Figure 20 – Hot-spot analysis using probability results from the best MARS model. Results reported in Z score and grouped by significance (99th percentile, 95th percentile and not significant areas)

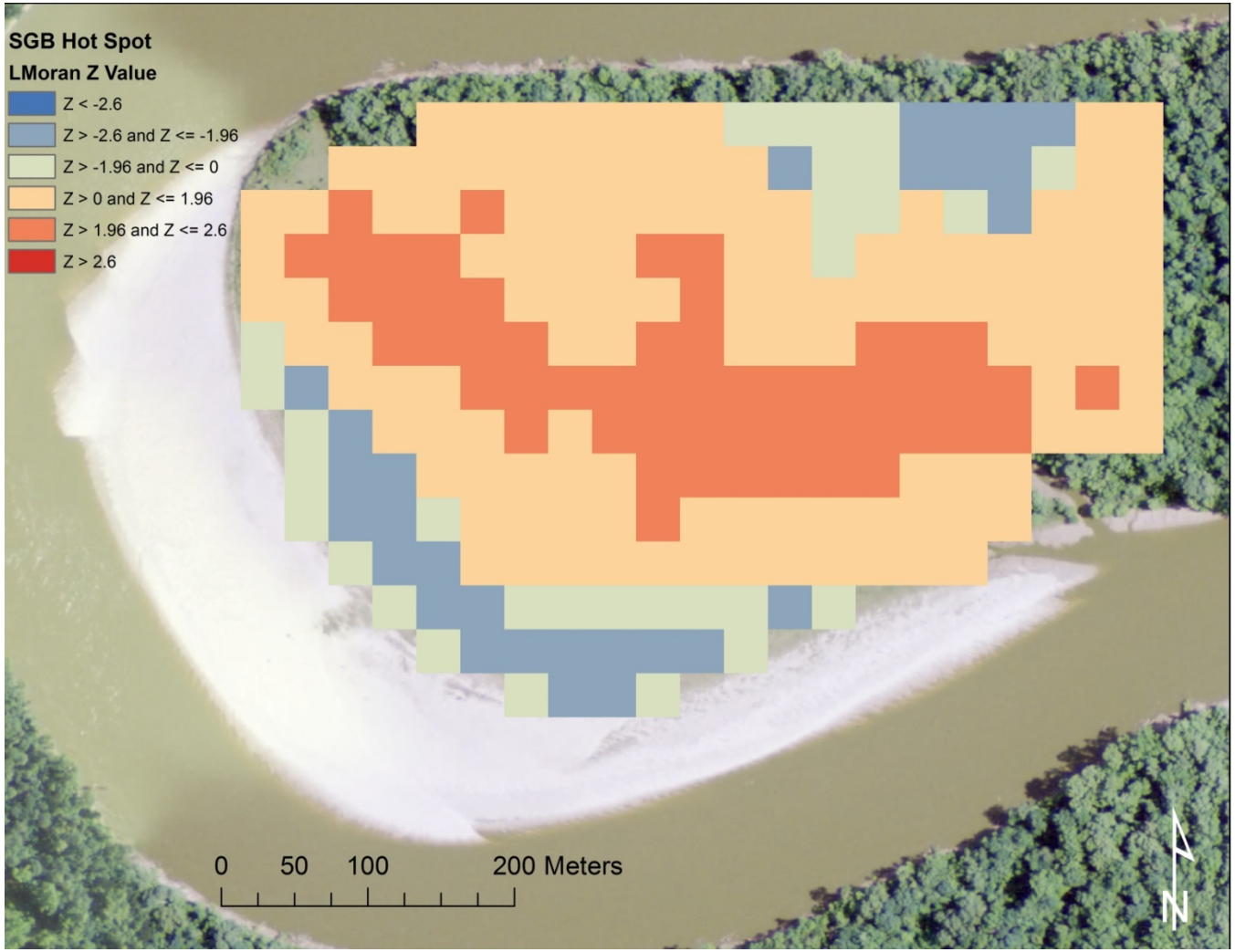

Figure 21 – Hot-spot analysis using probability results from the best SGB model. Results reported in Z score and grouped by significance (99th percentile, 95th percentile and not significant areas)

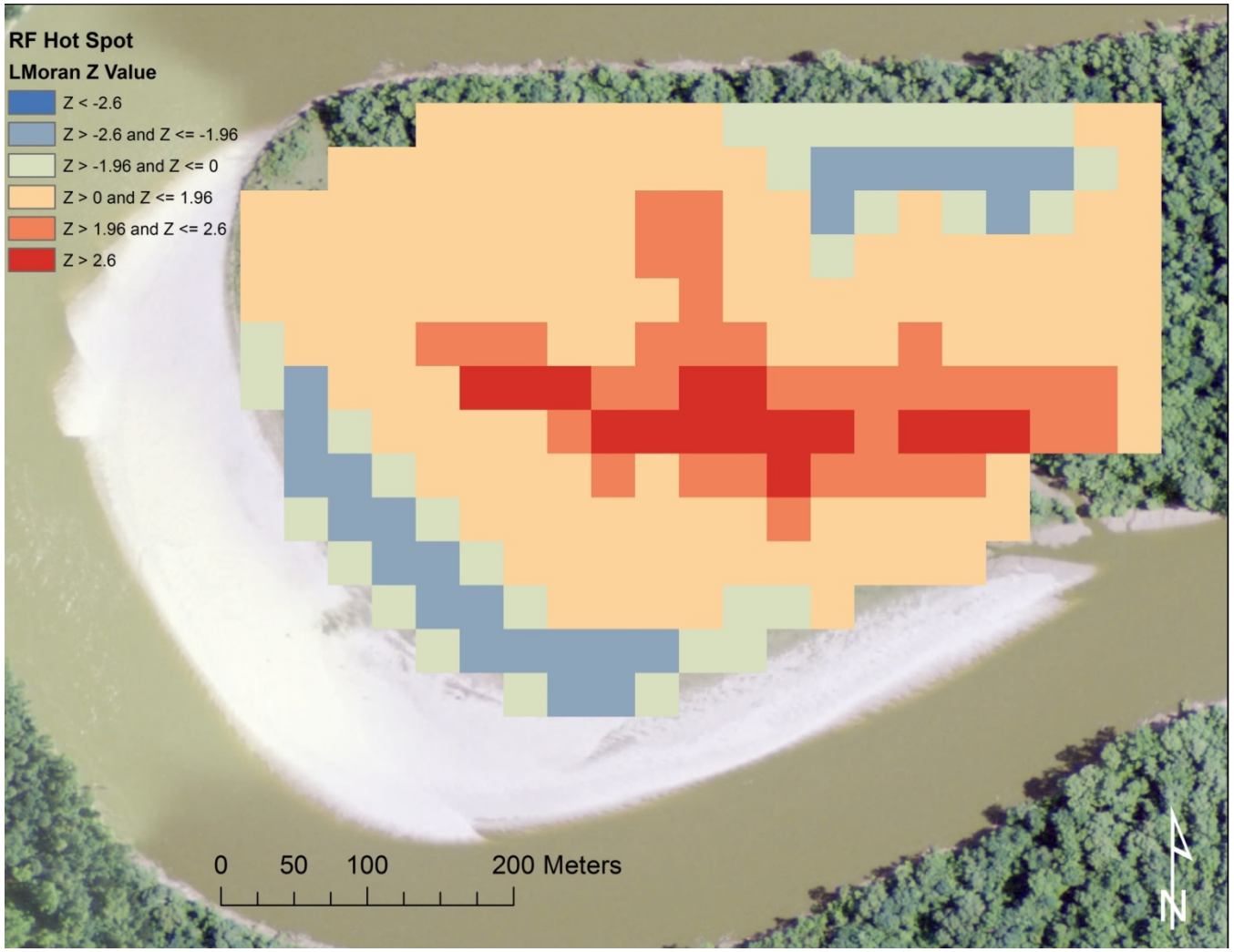

Figure 22 – Hot-spot analysis using probability results from the best RF model. Results reported in Z score and grouped by significance (99th percentile, 95th percentile and not significant areas)

5.6 Nonparametric model statistical comparison

5.6.1 McNemar statistical test

Binary comparisons are given in Tables 12-14 between the classification results of RF (trial 19), SGB (trial 19) and MARS (trial 5). Pairwise comparisons between algorithms showed there is no significant difference in the marginal distributions ($p < 0.001$) between the classification results of RF and SGB, p-value of 0.227, between MARS and RF, p-value of 0.581, and between SGB and MARS p-value of 0.687.

These results suggest that each of the algorithms is getting similar testing results, whether those results are correct or incorrect classifications. This may suggest that each of these algorithms is performing relatively similar at classifying certain parts of the image but may also be similarly performing poorly in other parts. While this may infer that all the algorithms are performing the same it does not really inform which of the models is performing differently from the others. Since the classification accuracies are relatively high, it does instill confidence that each of the algorithms may be suitable for classifying tallow.

	Random Forest Trial 19	
SGB Trial 19	0	1
0	26	3
1	8	33

Table 12- SGB trial 19 & Random Forest trial 19 confusion matrix

	MARS Trial 5	
Random Forest Trial 19	0	1
0	26	8
1	5	31

Table 13 - Random Forest trial 19 & MARS trial 5 confusion matrix

	MARS Trial 5	
SGB Trial 19	0	1
0	27	2
1	4	37

Table 14 - SGB trial 19 & MARS trial 5 confusion matrix

5.6.2 KAPPA analysis

In addition to the McNemar test a more traditional KAPPA analysis was performed (Congalton 1991). The KAPPA test reports whether or not each classification is better than a random classification to a statistically significant degree, in this case a 99% confidence level. The large Z statistic for each statistical test (Table 13) signifies that all three tests were more significant than a random classification (H_0 : K=0). This matches with previous results showing relatively high accuracy percentages.

Pairwise comparisons between the three error matrices for each test yielded results that differ from the McNemar results. Table 14 indicates through the z-statistic that there is a significant difference between the random forest and MARS results as well as the random forest and SGB results. The MARS and

SGB results do not have a significant difference. Given the overall accuracy results of the models this is more in line with what would be expected. This again emphasizes the utility of the MARS and SGB models, they may be more robust and accurate than a more typical random forest model.

Classification algorithm	KHAT statistic	Lower limit	Upper limit	Z Statistic	Variance	Result
RF Ex 19	0.59836	0.41025	0.78647	6.23462	0.00921	S
MARS Ex 5	0.85477	0.73216	0.97738	13.66409	0.00391	S
SGB Ex 19	0.85356	0.72993	0.97718	13.532	0.00397	S

Table 15 - KAPPA analysis test of significance for individual error matrices from the classification trials. S = significant result at the 99% confidence level. NS = non-significant results at the 95% confidence level

Pairwise comparison	Z Statistic	Result
RF Ex 19 and MARS Ex 5	-2.2382	S
RF Ex 19 and SGB Ex 19	-2.221	S
MARS Ex 5 and SGB Ex 19	0.0137	NS

Table 16 - Test for significant differences between error matrices

It is unclear why the KAPPA and McNemar test results are different but one hypothesis is that the tests are slightly different in design. The KAPPA test uses the confusion matrices as an input, whereas the McNemar uses the individual test results at each point and compares those results across the three

algorithms. In addition some of the literature (Foody and Mathur 2004) mentions that the McNemar test may not perform as well with a small sample size, and relatively small sample size is used in this study. The KAPPA results seem to be the more expected results and follow more closely with other statistical outputs for each individual model type. As concluded before, the MARS and SGB models seem to yield the best results.

6. DISCUSSION

The results achieved from the nonparametric models indicate that it is possible to map Chinese tallow. However using strictly presence and absence data in this study has most likely led to over-prediction of the presence of tallow and does not give a great representation of the density of tallow in the locations it has been predicted to be in. This also is partly due to using a 0.5 cutoff value for most of the models. This was the default within the modeling software and also was used in another study and so it was decided to use it in this research as well.

Using a .5 cutoff and using even one instance of tallow as a presence pixel may have had more of an effect on the SGB and RF results. The SGB and RF probability results (Figures 10 and 14) showed a distinct bimodal distribution with most values grouping near 0 and 1. While this type of distribution allows for a more accurate hard cutoff prediction it does not highlight areas where tallow has a moderate chance of being present. These areas may be those areas where tallow has colonized more recently or they may be more susceptible to tallow invasion in the near future. Because RF and SGB did not seem to do a good job at predicting these areas, it may be recommended that these methods be used more for tallow detection and not prediction.

MARS is the one nonparametric modeling method that may have been able to better predict these areas of possible or new tallow growth. The probability results from MARS (Figure 12) showed a larger range of values

across the study site yet still had strong values in those areas that have large amounts or no tallow. Because of that, it is recommended that MARS may be the most ideal method for modeling and predicting tallow growth in these riparian areas.

One of the primary reasons MARS may have performed better is because it is a fundamentally different model than RF and SGB. It does not make use of the decision tree structure, but rather uses a regression-based method which appears to be more useful in this situation. The downside of MARS in this particular context is that it cannot be used in a classification that is not Boolean, it can only classify a binary classification as was done in this study. The success of MARS may suggest that other regression-based techniques such as a generalized linear model, or a generalized additive model may perform well in this type of study as well.

Regarding the utility of the predictor variables, the vegetation indices tended to result in poor classification performance across all algorithms. Consistently across all classification algorithms, including those where other variables besides the indices were used, the four experiments involving the vegetation indices tend to have some of the lowest values among all of the statistical/accuracy metrics.

RF and MARS models developed in trial 5, where only the MNF bands were used as input variables, were among the most accurate models developed via those algorithms. In the MARS and SGB trials, the IC image

variables also produced high classifications accuracies when paired with either the geomorphometric variable group (in the case of SGB) or the AGB and soil predictors (in the case of MARS). It is important to note that while the geomorphometric, AGB and soil predictors never performed the best on their own, there are various trials that only yield good accuracies when using those variable groups in concert with the image-derived variables.

The RF baseline algorithm, compared with MARS and SGB, is not as accurate of an overall model predictor for the binary Chinese tallow-detection problem however it did prove to do best at classifying areas with low tallow (Tables 10 and 11). For these trials in this problem domain, MARS was not able to effectively perform classifications that are contain more than 2 classes and can only model binary classifications. SGB does have the capability of handling more robust classification problems because of its iterative nature and use of pseudo residuals and in this case should be regarded as the more robust and correct method for this problem, and most likely other classification problems as it had the highest overall accuracy results (Table 9) along with MARS (Table 10).

Overall, the results achieved from the nonparametric classification algorithms are positive and tend to reflect the observed distribution of Chinese tallow (Figure 5). Future studies may want to obtain more unbiased in-situ data to truly reflect the whole of the study area. In addition, this study could have benefited from knowing the amount of tallow at field sties in relation to amount of other species in the field plot. This information was only known for some of the

in-situ data collected and therefore could not be modeled. Regardless these results show confidence in all of the algorithms for producing accurate results with SGB and MARS outperforming RF.

However, when predicting areas with low percentages of tallow RF outperformed the other two algorithms when plots with no tallow were or were not included (Tables 10 and 11). When not including sites with no tallow the percentages for all algorithms are fairly low, this is most likely due to the low number of samples in the analysis. This statistical analysis suggest that RF is still a viable method and may perform better at predicting areas of low tallow which may be important for managers wanting to mitigate tallow early to avoid economic loss (Wang et al. 2012).

More extensive *in situ* data may have been able to improve the data and allowed for a more robust model. Instead of using just presence and absence, it would be better to use a model that incorporates percentage tallow at each site and thus better predict tallow in these areas. It would be better to have probability values that could relate directly to the percent abundance in a specific pixel. While that was the goal of this study, it cannot be said with certainty that the results achieved are representative of the percent abundance at the pixel level. MARS is the one model that may have been better at that kind of a prediction.

As this is the first study to use these nonparametric-modeling methods to detect/classify Chinese tallow, it is optimistic to view that the statistics and model

outputs generally follow the established patterns of tallow growth viewed throughout the study area. This research shows the value of using these model types for modeling not only tallow but possibly other invasive species in this type of riparian environment.

Of all the analyses performed for this research, the spectral analysis produced some of the more inconclusive results. SFF and SAM both produced underwhelming results although the SAM was able to predict general patterns of tallow growth on the point bar. The MTMF results which were expected to perform best were only able to pick out the areas with really high tallow growth.

A few things may be to blame for the weak spectral analysis results. The 30 meter spatial resolution is definitely an obstacle when performing this kind of analysis in the summer and in a small study area. When looking for end-members there was not a very distinct separation between different species in the study area. It is very difficult in such a heavily forested area to filter out the different end-members for different species. Although there is a pixel in the study area that is almost entirely composed of tallow the tallow end-member derived from this one pixel most likely was not sufficient to get a true separation of end-members when the various spectral methods were computed.

The field spectra were also not of a suitable quality to be used in the spectral analysis. There are a variety of factors that could have led to this. The spectra were not taken directly in the field and this may have led to false spectral readings when the spectra were shot in the lab. The leaves used for the spectra

may have not been preserved well enough. The lab spectra for Chinese tallow were averaged across all of the study sites that tallow spectra were collected from, this may have introduced some errors into the final lab spectra. If spectral analyses are to be used to detect tallow they most likely will need to employ the same strategy that Ramsey III did and use spectra and imagery from the fall months when tallow is senescing (Ramsey III and Nelson 2005a, Ramsey III et al. 2005c, Ramsey III et al. 2005b).

While it is more difficult to obtain and more expensive it is recommended that higher resolution hyperspectral imagery be used in future studies of this nature. If the study species is not grouped in larger stands, then it is difficult to obtain a pure spectra for the study species and thus difficult to unmix the pixel and determine the abundance in each of the pixels in the image. Other studies utilizing hyperspectral imagery have found success even with semi-moderate resolution of 10 or 15 meters (Underwood et al. 2003, Ustin et al. 2002, Filippi et al. 2014).

The hot-spot analyses hightlight where there are statistically-signficant hotspots of tallow or no tallow in the study area. The area along the chute cut is a hotspot for tallow, whereas the point bar and the more dense forest contain hotspots where there is no tallow. Many of these hotspots are significant at the 0.01 or 0.05 level. Although the hotspot results are good they do not emphasize much the interaction between Chinese tallow and other predictive variables but rather, just highlight cohesive areas that may contain tallow or do not contain

tallow to a high-degree of confidence. The spatial analysis portion of the research should be expanded in further research in order to truly link Chinese tallow growth with other predictive characteristics.

The study area used for this research is fairly small and localized. It will be of use to determine if the models and methods used in this study can be scaled up to predict tallow presence in a bigger area. The models used in this research may be used to model other larger riparian areas, particularly along the Trinity River. These models will most likely not work in other areas that are not riparian in nature, but these methods can be applied in those areas. Results will vary but these methods have shown their utility in this study.

7. CONCLUSIONS

As with many invasive species, Chinese tallow exhibits a marked ability to grow in varied environments, though its presence is more limited in certain portions of the study area. Results of this research indicate that Chinese tallow trees can be accurately detected in the summer using various remote-sensing methods.

The objectives of this research were: 1) to detect and map Chinese tallow in a floodplain forest using summer hyperspectral satellite image and other data, as well as nonparametric modeling and spectral unmixing/matching techniques; 2) to determine algorithm/dataset combinations that yield the highest-accuracy Chinese tallow classifications, of the detection algorithms and input variables tested; and 3) to quantitatively characterize the spatial distribution of Chinese tallow trees. This study is, to our knowledge, the first of its kind in that it attempts to detect Chinese tallow using remotely-sensed imagery acquired during summer months, and not to exploit spectral differences between senescent and non-senescent vegetation in the fall. Significantly, the proposed methodology, based on image data where vegetation is not senescing, thus geographically extends potential Chinese tallow-detection capability to areas where the leaves of many native tree species actually change from green to other colors during the fall, which complicates discrimination between Chinese tallow and native tree species during the fall season.

Nonparametric methods were found to be successful in mapping Chinese tallow presence. Only MARS was able to effectively produce a probability map that may indicate somewhat accurate probabilities, whereas SGB and RF seemed to only produce good hard classification maps. Utilizing hyperspectral imagery to map tallow using spectral unmixing methods was not entirely successful however, this is most likely due to the fact that it is difficult to obtain a good Chinese tallow endmember using an image with a coarse spatial resolution that was taken in the summer and contains a dense deciduous forest. Mixture tuned matched filtering was able to detect the tallow hotspot in the point bar but did not do well at predicting tallow at other areas of the point bar.

Spatial analysis was able to determine hotspots of tallow and non-tallow growth and to possibly intimate some of the factors that may drive tallow growth, namely geomorphometric and soil characteristics. These characteristics do not necessarily control the growth and spread of tallow but they may have more of an effect than other characteristics of the environment.

Future research that shows promise is utilizing available LiDAR data to attempt to map Chinese tallow. Using a dense high quality point cloud it may be possible to detect more of the tallow that is located in the understory of the canopy. One of the disadvantages of spectral remote sensing in dense forests is that it cannot give information about the understory and this is where much of the tallow outside of the transitional zone. LiDAR may be able to detect more of

that tallow and should be pursued as another method of mapping Chinese tallow.

Chinese tallow is a concerning invasive species in the southeastern United States and continues to spread and reduce biodiversity all throughout the region. Being able to track and map it is of importance as managers seek to control and mitigate the spread of tallow. Remote sensing may provide a cheap and efficient way to aid these managers by tracking tallow remotely. As of now only Ramsey III and collaborators have been able to accurately delineate tallow from other vegetation. However, that solution is dependent on the timing of the image-acquisition, and the processing was relatively intensive. While this research also is somewhat advanced, it contains concepts that managers may be able to eventually employ in order to map tallow.

REFERENCES

Andrew, M. E. & S. L. Ustin (2008) The role of environmental context in mapping invasive plants with hyperspectral image data. *Remote Sensing of Environment,* 112**,** 4301-4317.

Andrew, M. E. & S. L. Ustin (2009) Habitat suitability modelling of an invasive plant with advanced remote sensing data. *Diversity and Distributions,* 15**,** 627-640.

Beven, K. & M. Kirkby (1979) A physically based, variable contributing area model of basin hydrology/Un modèle à base physique de zone d'appel variable de l'hydrologie du bassin versant. *Hydrological Sciences Journal,* 24**,** 43-69.

Boardman, J. (1998) Leveraging the high dimensionality of AVIRIS data for improved subQpixel target unmixing and rejection of false positives: mixure tuned matched filtering. In *Summaries of the Seventh Annual JPL Airborne Geoscience Workshop*. Pasadena, CA.

Brandtberg, T., T. A. Warner, R. E. Landenberger & J. B. McGraw (2003) Detection and analysis of individual leaf-off tree crowns in small footprint, high sampling density lidar data from the eastern deciduous forest in North America. *Remote Sensing of Environment,* 85**,** 290-303.

Breiman, L. (2001) Random forests. *Machine learning,* 45**,** 5-32.

Breiman, L., J. H. Friedman, R. A. Olshen & C. J. Stone (1984) Classification and regression trees. Wadsworth & Brooks. *Monterey, CA*.

Brenning, A. (2009) Benchmarking classifiers to optimally integrate terrain analysis and multispectral remote sensing in automatic rock glacier detection. *Remote Sensing of Environment,* 113**,** 239-247.

Bruce, K. A., G. N. Cameron & P. A. Harcombe (1995) Initiation of a New Woodland Type on the Texas Coastal Prairie by the Chinese Tallow Tree (Sapium sebiferum (L.) Roxb.). *Bulletin of the Torrey Botanical Club,* 122**,** 215-225.

Burns, J. H. & T. E. Miller (2004) Invasion of Chinese Tallow (Sapium sebiferum) in the Lake Jackson area, Northern Florida. *The American Midland Naturalist,* 152**,** 410-417.

Butterfield, B. J., W. E. Rogers & E. Siemann (2004) Growth of Chinese tallow tree (Sapium sebiferum) and four native trees under varying water regimes. *Texas Journal of Science,* 56**,** 335-347.

Camporeale, C. & L. Ridolfi (2006) Riparian vegetation distribution induced by river flow variability: A stochastic approach. *Water Resources Research,* 42.

Camporeale, C. & L. Ridolfi (2010) Interplay among river meandering, discharge stochasticity and riparian vegetation. *Journal of Hydrology,* 382**,** 138-144.

Carlson, T. N. & D. A. Ripley (1997) On the relation between NDVI, fractional vegetation cover, and leaf area index. *Remote sensing of Environment,* 62**,** 241-252.

Chambless, L. & E. Nixon (1975) Woody vegetation--soil relations in a bottomland forest of east Texas. *Texas Journal of Science*.

Cho-ying, H. & G. P. Asner (2009) Applications of Remote Sensing to Alien Invasive Plant Studies. *Sensors (14248220),* 9**,** 4869-4889.

Clark, R. N. & G. A. Swayze (1995) Mapping minerals, amorphous materials, environmental materials, vegetation, water, ice, and snow, and other materials: The USGS Tricorder Algorithm. In *Summaries of the Fifth Annual JPL Airborne Earth Science Workshop*, 39-40. JPL Publication.

Congalton, R. G. (1991) A review of assessing the accuracy of classifications of remotely sensed data. *Remote Sensing of Environment,* 37**,** 35-46.

Cooper, D. J., D. C. Andersen & R. A. Chimner (2003) Multiple pathways for woody plant establishment on floodplains at local to regional scales. *Journal of Ecology,* 91**,** 182-196.

Coppin, P. R. & M. E. Bauer (1996) Digital change detection in forest ecosystems with remote sensing imagery. *Remote Sensing Reviews,* 13**,** 207-234.

Correll, D. S. & M. C. Johnston (1970) Manual of the vascular plants of Texas. *Contributions from Texas Research Foundation. A series of botanical studies,* 6.

Cutler, D. R., T. C. Edwards, K. H. Beard, A. Cutler, K. T. Hess, J. Gibson & J. J. Lawler (2007) Random Forests for Classification in Ecology. *Ecology,* 88**,** 2783-2792.

Datt, B. (1999) A New Reflectance Index for Remote Sensing of Chlorophyll Content in Higher Plants: Tests using Eucalyptus Leaves. *Journal of Plant Physiology,* 154**,** 30-36.

Duro, D. C., S. E. Franklin & M. G. Dubé (2012) A comparison of pixel-based and object-based image analysis with selected machine learning algorithms for the classification of agricultural landscapes using SPOT-5 HRG imagery. *Remote Sensing of Environment,* 118**,** 259-272.

Elith, J., J. R. Leathwick & T. Hastie (2008) A working guide to boosted regression trees. *Journal of Animal Ecology,* 77**,** 802-813.

Filippi, A. M., İ. Güneralp & J. Randall (2014) Hyperspectral remote sensing of aboveground biomass on a river meander bend using multivariate adaptive regression splines and stochastic gradient boosting. *Remote Sensing Letters***,** 432-441.

Filippi, A. M. & J. R. Jensen (2006) Fuzzy learning vector quantization for hyperspectral coastal vegetation classification. *Remote Sensing of Environment,* 100**,** 512-530.

Foody, G. M. & A. Mathur (2004) A relative evaluation of multiclass image classification by support vector machines. *Geoscience and Remote Sensing, IEEE Transactions on,* 42**,** 1335-1343.

Friedman, J. H. (1991) Multivariate Adaptive Regression Splines. *The Annals of Statistics,* 19**,** 1-67.

Friedman, J. H. (2002) Stochastic gradient boosting. *Computational Statistics & Data Analysis,* 38**,** 367-378.

Gamon, J., J. Penuelas & C. Field (1992) A narrow-waveband spectral index that tracks diurnal changes in photosynthetic efficiency. *Remote Sensing of Environment,* 41**,** 35-44.

Gamon, J. & J. Surfus (1999) Assessing leaf pigment content and activity with a reflectometer. *New Phytologist,* 143**,** 105-117.

Gan, J., J. H. Miller, H. Wang & J. W. Taylor (2009) Invasion of tallow tree into southern US forests: influencing factors and implications for mitigation. *Canadian Journal of Forest Research,* 39**,** 1346-1356.

Gitelson, A. A. & M. N. Merzlyak (1996) Signature analysis of leaf reflectance spectra: algorithm development for remote sensing of chlorophyll. *Journal of Plant Physiology,* 148**,** 494-500.

Godfrey, R. K. (1988) *Trees, shrubs, and woody vines of northern Florida and adjacent Georgia and Alabama*. University of Georgia Press.

Green, A. A., M. Berman, P. Switzer & M. D. Craig (1988) A transformation for ordering multispectral data in terms of image quality with implications for noise removal. *Geoscience and Remote Sensing, IEEE Transactions on,* 26**,** 65-74.

Groeneveld, D. P. & R. P. Watson (2008) Near-infrared discrimination of leafless saltcedar in wintertime Landsat TM. *International Journal of Remote Sensing,* 29**,** 3577-3588.

Güneralp, İ., A. M. Filippi & B. Hales (2014a) Influence of river channel morphology and bank characteristics on water surface boundary delineation using high-resolution passive remote sensing and template matching. *Earth Surface Processes and Landforms,* 39**,** 977-986.

Güneralp, İ., A. M. Filippi & B. U. Hales (2013) River-flow boundary delineation from digital aerial photography and ancillary images using Support Vector Machines. *GIScience & Remote Sensing,* 50**,** 1-25.

Güneralp, İ., A. M. Filippi & J. Randall (2014b) Estimation of floodplain aboveground biomass using multispectral remote sensing and nonparametric modeling. *International Journal of Applied Earth Observation and Geoinformation,* 33**,** 119-126.

Güneralp, İ. & B. L. Rhoads (2009) Empirical analysis of the planform curvature-migration relation of meandering rivers. *Water Resources Research,* 45.

Güneralp, İ. & B. L. Rhoads (2010) Spatial autoregressive structure of meander evolution revisited. *Geomorphology,* 120**,** 91-106.

Güneralp, İ. & B. L. Rhoads (2011) Influence of floodplain erosional heterogeneity on planform complexity of meandering rivers. *Geophysical Research Letters,* 38.

Hestir, E. L., S. Khanna, M. E. Andrew, M. J. Santos, J. H. Viers, J. A. Greenberg, S. S. Rajapakse & S. L. Ustin (2008) Identification of invasive vegetation using hyperspectral remote sensing in the California Delta ecosystem. *Remote Sensing of Environment,* 112**,** 4034-4047.

Howes, F. N. (1949) The Chinese Tallow Tree (Sapium sebiferum Roxb.): A Source of Drying Oil. *Kew Bulletin,* 4**,** 573-580.

Huang, C. & J. R. G. Townshend (2003) A stepwise regression tree for nonlinear approximation: Applications to estimating subpixel land cover. *International Journal of Remote Sensing,* 24**,** 75-90.

Huber, P. J. (2011) *Robust statistics*. Springer.

Hupp, C. R. & W. R. Osterkamp (1996) Riparian vegetation and fluvial geomorphic processes. *Geomorphology,* 14**,** 277-295.

Hyvärinen, A., J. Karhunen & E. Oja (2004) *Independent Component Analysis*. John Wiley & Sons.

SPSS Statistics for Windows. Version 22.0, IBM Corp., Armonk, NY.

ACORN 5.0 User's Manual. Version 040801, ImSpec LLC.

ENVI User's Guide. Boulder, CO:ITT - Visual Information Solutions.

Jensen, J. R. (1996) *Introductory Digital Image Processing: A Remote Sensing Perspective*. Prentice-Hall Inc.

Jubinsky, G. & L. C. Anderson (1996) The Invasive Potential of Chinese Tallow-Tree (Sapium sebiferum Roxb.) in the Southeast. *Castanea,* 61**,** 226-231.

Kaufman, Y. J. & D. Tanré (1996) Strategy for direct and indirect methods for correcting the aerosol effect on remote sensing: from AVHRR to EOS-MODIS. *Remote Sensing of Environment,* 55**,** 65-79.

Latifi, H., A. Nothdurft & B. Koch (2010) Non-parametric prediction and mapping of standing timber volume and biomass in a temperate forest: application of multiple optical/LiDAR-derived predictors. *Forestry,* 83**,** 395-407.

Lawrence, R. L., S. D. Wood & R. L. Sheley (2006) Mapping invasive plants using hyperspectral imagery and Breiman Cutler classifications (randomForest). *Remote Sensing of Environment,* 100**,** 356-362.

Leathwick, J. R., J. Elith & T. Hastie (2006) Comparative performance of generalized additive models and multivariate adaptive regression splines for statistical modelling of species distributions. *Ecological Modelling,* 199**,** 188-196.

Mellor, A., A. Haywood, C. Stone & S. Jones (2013) The performance of random forests in an operational setting for large area sclerophyll forest classification. *Remote Sensing,* 5**,** 2838-2856.

Moisen, G. G., E. A. Freeman, J. A. Blackard, T. S. Frescino, N. E. Zimmermann & T. C. Edwards Jr (2006) Predicting tree species presence and basal area in Utah: A comparison of stochastic gradient boosting, generalized additive models, and tree-based methods. *Ecological Modelling,* 199**,** 176-187.

Moisen, G. G. & T. S. Frescino (2002) Comparing five modelling techniques for predicting forest characteristics. *Ecological Modelling,* 157**,** 209-225.

Muñoz, J. & Á. M. Felicísimo (2004) Comparison of statistical methods commonly used in predictive modelling. *Journal of Vegetation Science,* 15**,** 285-292.

Nagendra, H., R. Lucas, J. P. Honrado, R. H. G. Jongman, C. Tarantino, M. Adamo & P. Mairota (2012) Remote sensing for conservation monitoring: Assessing protected areas, habitat extent, habitat condition, species diversity, and threats. *Ecological Indicators*.

Naiman, R. J., H. Decamps & M. E. McClain (2010) *Riparia: ecology, conservation, and management of streamside communities*. Academic Press.

Narumalani, S., D. R. Mishra, R. Wilson, P. Reece & A. Kohler (2009) Detecting and Mapping Four Invasive Species Along The Floodplain of North Platte River, Nebraska. *Weed Technology,* 23**,** 99-107.

Nijjer, S., R. A. Lankau, W. E. Rogers & E. Siemann (2002) Effects of temperature and light on Chinese tallow (Sapium sebiferum) and Texas sugarberry (Celtis laevigata) seed germination. *Texas Journal of Science,* 54**,** 63-68.

Nyikos, S. I. (2011) Tree Community Patterns and Soil Texture Characteristics of a Meander Bend, Lower Trinity River, Southeast Texas. Texas A&M University.

Pattison, R. & R. Mack (2009) Environmental constraints on the invasion of Triadica sebifera in the eastern United States: an experimental field assessment. *Oecologia,* 158**,** 591-602.

Pengra, B. W., C. A. Johnston & T. R. Loveland (2007) Mapping an invasive plant, Phragmites australis, in coastal wetlands using the EO-1 Hyperion hyperspectral sensor. *Remote Sensing of Environment,* 108**,** 74-81.

Penuelas, J., F. Baret & I. Filella (1995) Semi-empirical indices to assess carotenoids/chlorophyll a ratio from leaf spectral reflectance. *Photosynthetica,* 31**,** 221-230.

Perucca, E., C. Camporeale & L. Ridolfi (2007) Significance of the riparian vegetation dynamics on meandering river morphodynamics. *Water Resources Research,* 43.

Phillips, J. D. (1992) Nonlinear dynamical systems in geomorphology: revolution or evolution? *Geomorphology,* 5**,** 219-229.

Planty-Tabacchi, A.-M., E. Tabacchi, R. J. Naiman, C. Deferrari & H. Décamps (1996) Invasibility of Species-Rich Communities in Riparian Zones: La propensión a la invasión de las comunidades de zonas ribereñas ricas en especies. *Conservation Biology,* 10**,** 598-607.

Prasad, A., L. Iverson & A. Liaw (2006) Newer Classification and Regression Tree Techniques: Bagging and Random Forests for Ecological Prediction. *Ecosystems,* 9**,** 181-199.

Pysek, P. & K. Prach (1993) Plant Invasions and the Role of Riparian Habitats: A Comparison of Four Species Alien to Central Europe. *Journal of Biogeography,* 20**,** 413-420.

QGIS Geographic Information System. Open Source Geospatial Foundation Project.

Ramsey III, E. & G. Nelson (2005a) A whole image approach using field measurements for transforming EO1 Hyperion hyperspectral data into canopy reflectance spectra. *International Journal of Remote Sensing,* 26**,** 1589-1610.

Ramsey III, E., G. A. Nelson, S. K. Sapkota, E. B. Seeger & K. D. Martella (2002) Mapping Chinese tallow with color-infrared photography. *Photogrammetric Engineering & Remote Sensing,* 68**,** 251-255.

Ramsey III, E., A. Rangoonwala, G. Nelson & R. Ehrlich (2005c) Mapping the invasive species, Chinese tallow, with EO1 satellite Hyperion hyperspectral image data and relating tallow occurrences to a classified Landsat Thematic Mapper land cover map. *International Journal of Remote Sensing,* 26**,** 1637-1657.

Ramsey III, E., A. Rangoonwala, G. Nelson, R. Ehrlich & K. Martella (2005b) Generation and validation of characteristic spectra from EO1 Hyperion image data for detecting the occurrence of the invasive species, Chinese tallow. *International Journal of Remote Sensing,* 26**,** 1611-1636.

Richardson, D. M., P. M. Holmes, K. J. Esler, S. M. Galatowitsch, J. C. Stromberg, S. P. Kirkman, P. Pyšek & R. J. Hobbs (2007) Riparian vegetation: degradation, alien plant invasions, and restoration prospects. *Diversity and Distributions,* 13**,** 126-139.

Robertson, K. M. & C. K. Augspurger (1999) Geomorphic processes and spatial patterns of primary forest succession on the Bogue Chitto River, USA. *Journal of Ecology,* 87**,** 1052-1063.

Rogers, W. E. & E. Siemann (2003) Effects of simulated herbivory and resources on Chinese tallow tree (Sapium sebiferum, Euphorbiaceae) invasion of native coastal prairie. *American Journal of Botany,* 90**,** 243-249.

Rosenberg, D. M., P. McCully & C. M. Pringle (2000) Global-Scale Environmental Effects of Hydrological Alterations: Introduction. *BioScience,* 50**,** 746-751.

Rouse, J. (1974) Monitoring vegetation systems in the Great Plains with ERTS. In *NASA. Goddard Space Flight Center 3 d ERTS-1 Symp*.

Salford Predictive Modeler. Salford Systems, San Diego, CA.

Shafroth, P. B., J. C. Stromberg & D. T. Patten (2002) Riparian Vegetation Response to Altered Disturbance and Stress Regimes. *Ecological Applications,* 12**,** 107-123.

Shepherd, K. D. & M. G. Walsh (2002) Development of Reflectance Spectral Libraries for Characterization of Soil Properties. *Soil Sci. Soc. Am. J.,* 66**,** 988-998.

Sher, A. A., D. L. Marshall & S. A. Gilbert (2000) Competition between native Populus deltoides and invasive Tamarix ramosissima and the implications for reestablishing flooding disturbance. *Conservation Biology,* 14**,** 1744-1754.

Stohlgren, T. J., P. Ma, S. Kumar, M. Rocca, J. T. Morisette, C. S. Jarnevich & N. Benson (2010) Ensemble Habitat Mapping of Invasive Plant Species. *Risk Analysis,* 30**,** 224-235.

Suits, G. H. (1973) The calculation of the directional reflectance of a vegetative canopy. *Remote Sensing of Environment,* 2**,** 117-125.

Thébaud, C. & M. Debussche (1991) Rapid Invasion of Fraxinus ornus L. Along the Hérault River System in Southern France: The Importance of Seed Dispersal by Water. *Journal of Biogeography,* 18**,** 7-12.

Torresan, C. L., J. Strunk, H. S. Zald, Y. Zhiqiang & W. B. Cohen (2014) Comparing statistical techniques to classify the structure of mountain forest stands using CHM-derived metrics in Trento province (Italy).

Tucker, C. J. (1979) Red and photographic infrared linear combinations for monitoring vegetation. *Remote Sensing of Environment,* 8**,** 127-150.

Underwood, E., S. Ustin & D. DiPietro (2003) Mapping nonnative plants using hyperspectral imagery. *Remote Sensing of Environment,* 86**,** 150-161.

USDA, (2014) Plant Database: *Triadica sebifera*. USDA.gov.

Ustin, S. L., D. DiPietro, K. Olmstead, E. Underwood & G. J. Scheer (2002) Hyperspectral remote sensing for invasive species detection and mapping. In *Geoscience and Remote Sensing Symposium, 2002. IGARSS '02. 2002 IEEE International*, 1658-1660 vol.3.

van Coller, A. L., K. H. Rogers & G. L. Heritage (2000) Riparian vegetation-environment relationships: complimentarity of gradients versus patch hierarchy approaches. *Journal of vegetation science,* 11**,** 337-350.

Vitousek, P. M., C. M. D'Antonio, L. L. Loope, M. Rejmanek & R. Westbrooks (1997) Introduced species: a significant component of human-caused global change. *New Zealand Journal of Ecology,* 21**,** 1-16.

Vogelmann, J., B. Rock & D. Moss (1993) Red edge spectral measurements from sugar maple leaves. *TitleREMOTE SENSING,* 14**,** 1563-1575.

Wang, H.-H., W. E. Grant, J. Gan, W. E. Rogers, T. M. Swannack, T. E. Koralewski, J. H. Miller & J. W. Taylor (2012) Integrating spread dynamics and economics of timber production to manage Chinese tallow invasions in southern US forestlands. *PloS one,* 7**,** e33877.

Wang, H.-H., W. E. Grant, T. M. Swannack, J. Gan, W. E. Rogers, T. E. Koralewski, J. H. Miller & J. W. Taylor (2011) Predicted range expansion of Chinese tallow tree (Triadica sebifera) in forestlands of the southern United States. *Diversity and Distributions,* 17**,** 552-565.

Ward, R. W. (2002) Extent and dispersal rates of Chinese privet (Ligustrum sinense) invasion on the upper Oconee River floodplain, North Georgia. *Southeastern Geographer,* 42**,** 29-48.

Yuhas, R. H., A. F. Goetz & J. W. Boardman (1992) Discrimination among semi-arid landscape endmembers using the spectral angle mapper (SAM) algorithm. In *Summaries of the third annual JPL airborne geoscience workshop*, 147-149. Pasadena, CA: JPL Publication.

Zevenbergen, L. W. & C. R. Thorne (1987) Quantitative analysis of land surface topography. *Earth surface processes and landforms,* 12**,** 47-56.

Zou, J., W. E. Rogers, S. J. DeWalt & E. Siemann (2006) The effect of Chinese tallow tree (Sapium sebiferum) ecotype on soil–plant system carbon and nitrogen processes. *Oecologia,* 150**,** 272-281.

Zou, J., W. E. Rogers & E. Siemann (2009) Plasticity of Sapium sebiferum seedling growth to light and water resources: Inter-and intraspecific comparisons. *Basic and Applied Ecology,* 10**,** 79-88.